

University of Arkansas, Fayetteville  
**ScholarWorks@UARK**

---

Graduate Theses and Dissertations

---

5-2016

## Statistical Analysis of Fluvial Channel Belts

Kyle Ryan Spencer  
*University of Arkansas, Fayetteville*

Follow this and additional works at: <https://scholarworks.uark.edu/etd>



Part of the [Geology Commons](#), [Geomorphology Commons](#), and the [Sedimentology Commons](#)

---

### Citation

Spencer, K. R. (2016). Statistical Analysis of Fluvial Channel Belts. *Graduate Theses and Dissertations*  
Retrieved from <https://scholarworks.uark.edu/etd/1604>

This Thesis is brought to you for free and open access by ScholarWorks@UARK. It has been accepted for inclusion in Graduate Theses and Dissertations by an authorized administrator of ScholarWorks@UARK. For more information, please contact [scholar@uark.edu](mailto:scholar@uark.edu), [uarepos@uark.edu](mailto:uarepos@uark.edu).

Statistical Analysis of Fluvial Channel Belts

A thesis submitted in partial fulfillment  
of the requirements for the degree of  
Master of Science in Geology

By

Kyle Spencer  
Texas A&M University  
Bachelor of Science in Geology, 2013  
May 2016  
University of Arkansas

This thesis is approved for recommendation to the Graduate Council

---

Dr. John Shaw  
Thesis Director

---

Dr. Chris Liner  
Committee Member

---

Dr. Doy Zachry  
Committee Member

## Abstract

As meandering rivers laterally migrate over time, they build channel belts. The accumulation of all previous flow paths creates the channel belt. To better understand these ancient rivers, modern river systems are being mapped to find statistical relationships between current flow path and the channel belt of river systems. It is important to examine a wide range of systems in terms of age, size, and location. The rivers are being mapped using an ImageJ, interpretations from Saucier (1994) and Google Earth. Three channel belt morphologies are mapped for 15 modern channel belts; the width of the river in relation to the width of the channel belt; the curvature of the meander scars on the channel belt; and the spacing length between unconformable points. Unconformable points are locations where these previous flow paths overlap one another on the channel belt edge. Statistical analysis of the data reveals that the median range for the ratio of channel belt width to mean channel width ( $W^*$ ) is 8.9 to 76,  $W^*$  for the data set also as a  $P_{90}/P_{10}$  range of 1.6 to 3.7. The median range for the normalized radius of curvature of the channel belt ( $P^*$ ) for the entire data set is 3.8 to 35 and has a  $P_{90}/P_{10}$  range of 16 to 49. The median range for the normalized spacing between unconformable points ( $L^*$ ) for all river reaches in the data set is 2.7 to 24, with a  $P_{90}/P_{10}$  range of 2.9 to 7.6. These variation constraints provide information about the formation of fluvial channel belts and the petroleum reservoirs they can create.

©2016 by Kyle Spencer  
All Rights Reserved

## **Acknowledgements**

I first want to thank my advisor and committee chairman, Dr. John Shaw, for aligning me with this project and his guidance through this process. The support and energy you provided from start to finish of my Master's degree has been unmatched. You have led me to become a better academic who thinks outside the box. I also would like to thank my committee members, Dr. Doy Zachry and Dr. Christopher Liner, for all their recommendations, encouragement, and support through my time here at the University of Arkansas.

Next I would also like to thank my family. This project and journey would not have been possible without your unbridled support and encouragement, despite all the geology jokes.

I would also like to thank all of my close friends here and around the country for their continued support. I would like to thank the University Of Arkansas Geosciences Department for extending the opportunity to attend graduate school here. It has been a complete blessing.

## Table of Contents

1. Introduction	1
1.1 Objective	1
1.2 Motivation	1
1.3 Nomenclature	2
1.4 Literature Review	6
1.4.1 Jefferson (1902)	6
1.4.2 Leopold and Wolman (1960)	7
1.4.3 Alford and Holmes (1985)	9
1.4.4 Gibling (2006)	9
2. Data Location	10
2.1 Rivers	10
2.2 Lower Mississippi River Valley	13
2.3 Additional Rivers	15
3. Methodology	16
3.1 Workflow	16
3.2 Software Selection	17
3.3 Channel-Belt Identification	18
3.4 Measuring Techniques	22
3.5 Data Processing	24
4. Results	29
4.1 Channel Belt Width ( $W^*$ )	29
4.2 Spacing of Unconformable Points ( $L^*$ )	31

4.3 Radius of Curvature ( $P_{CB}^*$ )	32
4.4 $P_{90}/P_{10}$	33
4.5 Radius of Curvature (Channel Belt vs. Channel)	34
4.6 Relationships Between Channel Belt Morphology	35
5. Discussion	36
5.1 Channel Belt Width	36
5.2 Spacing of Unconformable Points	37
5.3 Radius of Curvature of Channel Belts and Channels	38
5.4 Angle $\alpha$	39
5.5 Future Work	40
6. Conclusions	40
6.1 Channel Belt Width	40
6.2 Spacing of Unconformable Points	40
6.3 Radius of Curvature on Channel Belt	43
6.4 Relationships Between Channel Belt Morphology and angle $\alpha$	41
Works Cited	42
Appendix 1 Table of Variables	44

## List of Figures

Figure 1: Cartoon formation of a channel belt simplified and zoomed in

Figure 2: Formation of channel belt elaborated

Figure 3: Map modified from Jefferson (1902) Speyer, Germany

Figure 4: Google Earth map illustrating locations of reaches in data set

Figure 5: Google Earth map of Selenga river reach in Russia

Figure 6: Workflow

Figure 7: Google Earth map of Muddy Creek reach highlighting channel belt

Figure 8: Plate 7 (Saucier 1994)

Figure 9: Holocene Units modified from (Saucier 1994)

Figure 10: Google Earth map illustrating measurements on Neches River reach

Figure 11: Meander angle arc alpha

Figure 12: Channel belt width ( $W^*$ ) CDF

Figure 13: Spacing of Unconformable Points ( $L^*$ ) CDF

Figure 14: Radius of Curvature ( $P^*$ ) CDF

Figure 15: Radius of Curvature (Channel Belt vs. Modern Channel)

## List of Charts

Table 1: Location of all river reaches within data set.

Table 2: Numbered reaches found in Figure 4 with associated reach

Table 3: P90/P10 values calculated for  $W^*$ ,  $L^*$ , and  $P^*$  for data set

Table 4: The median values for the calculations of  $W/P$ ,  $L/P$ ,  $W/L$ , and  $\alpha$



## **1. Introduction**

### **1.1 Objective**

The focus of this study is to discover statistical relationships and constraints of the channel belt morphology of meandering river systems. By measuring the planform channel belt morphology, from aerial imagery, and plotting measurements in cumulative distribution functions the statistical constraints can be revealed. This study also aims to develop replicable methods of data collection so more river reaches can be studied and so that this study can be examined in other ways in the future. This will be significant because it will allow exploration geologists to learn about river kinematics on a broad scale from preserved channel belts.

### **1.2 Motivation**

Ancient meandering river systems make for valuable oil and gas reservoirs (Martin 1993). The low gradients found in meandering river systems have high-suspended bed loads, which deposits great reservoir material as the river laterally migrates (Saucier 1994). The large amount of sediment that is deposited in point bars is what makes these systems ideal for creating petroleum reservoirs. The problem with understanding these reservoirs is that as these rivers meander; they create a complex stacking of deposits over time, which are difficult to track in outcrops (Martin 1993).

Comparing distributions of channel-belt width, radius of curvature for the lateral extent of the channel-belt, and the spacing of unconformable points is a new approach to fluvial stratigraphy. There have been many studies on the radius of meander bends both on the channel and the channel belt (Leopold and Wolman 1960; Alford and Holmes 1985; Limaye and Lamb 2014). Other studies focus on the channel belt width in relation to the channel width as well as the width to thickness ratio of the channel belt (Jefferson 1902; Gibling 2006). While plenty of

work has been done on these topics, they are not typically studied via a distribution of measurements. The distribution of measurements produces estimates about the river system's kinematics and channel belt evolution, which will benefit both stratigraphers and exploration geoscientists. Thanks to the advancements of 3-D seismic technology, these channel belts and geomorphic surfaces can be measured and interpreted in the subsurface (Martin 1993). To properly study these surfaces, analogues to modern systems are needed to understand the ancient systems (Figure 2C).

### **1.3 Nomenclature**

As lateral migration of channels occurs over time, the results leave erosional meander scars and depositional point bars. While “channel belts” are typically net-depositional features, net-erosional incised valleys share similar geometric patterns as their depositional counterparts (Blum and Törnqvist 2000; Blum, Morton, and Durbin 1995; Hickin and Nanson 1984; Hickin 1974). Therefore, this study defines the “channel belt” as the amalgamation of all surface morphology built from previous flow paths when viewed in planform projection. The planform geometry of channel belt morphology contains an incomplete yet compelling record of the kinematics of the meandering river.

The ratio between channel belt width and mean channel width,  $W^*$ , was the jumping off point for this study (appendix 1). The channel belt width is the lateral extent of a channel belt perpendicular to the general downstream trend of the belt. Similar ratios have been studied in the past. However, those studies are not as inclusive in their measurements or statistical analysis (Jefferson 1902). The lack of further research trying to recreate these findings is curious, especially given how frequently the study is cited. The distribution of  $W^*$  within a single channel belts or between channel belts was not discussed in previous studies (Jefferson 1902). In this

study, these variations will be explicitly resolved. I suspect the relationship between the channel-belt width and channel width is more complex and the variability even within a single river reach needs to be highlighted. These complexities create curiosity to find other features to study from aerial imagery.

The second aspect of channel belt morphology measured in this study was the radius of curvature on the edges of the channel belt and the current channel (Figure 1B). The radius of curvature,  $P$ , is the radius of a circle that lies tangent to the channel belt or modern channel (Appendix 1). Studying the radius of curvature is important because it is prominently preserved on the channel-belt and reveals new information for the river's kinematics and channel belt evolution. The radius of curvature of meander bends has been studied before, but typically meander bends are specifically selected in order to fit a theoretical equation (Leopold and Wolman 1960; Williams 1986). Williams (1986) combined data from other studies to collect a very large data set, however, he specifically took samples where (1) channels were alluvial, (2) sinuosity was  $\geq 1.20$ , and (3) shared similar measuring techniques. Other studies had to be specific in selecting reaches with a certain sinuosity because it used statistics from both real and simulated river systems (Stølum 1998). Many studies measure specific meander bends on the channel and channel-belt, most do not measure the entire extent of the river reach as is done in my study. Radius of curvature on the channel belt, for my study, was measured as a distribution for the entire length of the channel belt and not just for specific meander bend (Figure 2B). By measuring the radius of curvature as a distribution for the entire channel belt prevents a biasness that could occur by selecting specific meanders. The radius of curvature on the channel belt edge can be measured within a seismic volume that has had sweetness attributes applied (Figure 2C).

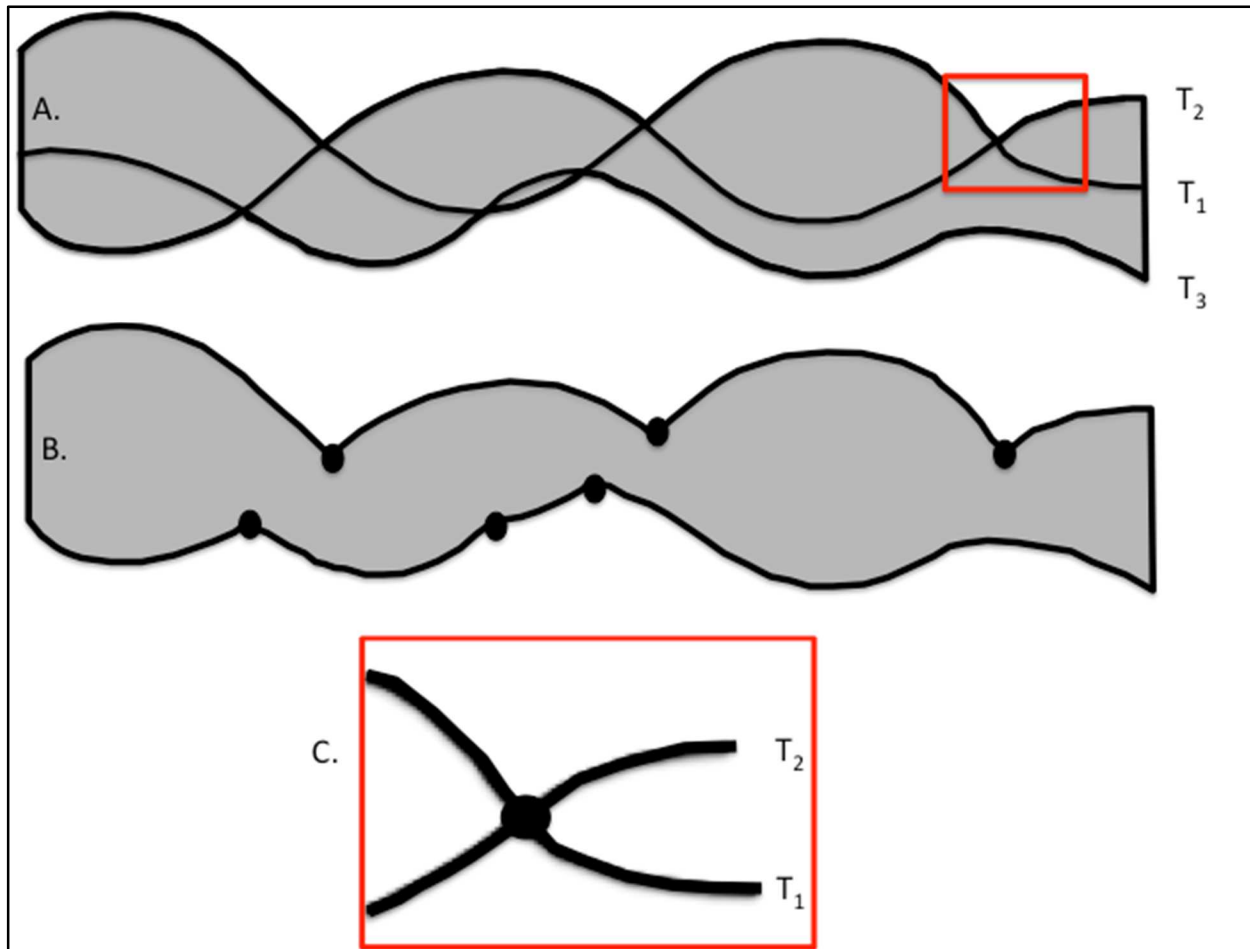


Figure 1: (A) Showing the progression and evolution of a channel-belt (gray) by three different flow paths  $T_1$ ,  $T_2$ , and  $T_3$  overlapping. (B) The channel belt (gray) created by flow paths  $T_1$ ,  $T_2$ , and  $T_3$  the points designated by the large black dots. (C) Inside the red box is a zoomed in view of the red box in (A) of an unconformable point (black dot) where path  $T_2$  crosses over the path  $T_1$  on the edge of the channel belt.

Time plays a major role in the creation of channel belts and the channel belt morphology shows previous flow paths caused by lateral migration over extended periods of time (Figure 1A & 2A). Where two differently aged channel courses overlap on the edge of the channel-belt it creates a depositional time gap and are being defined as unconformable points (Figure 1C & 2B). The last channel belt morphology investigated incorporates the time component in a completely new way is the spacing between unconformable points ( $L$ ) (Figure 1A)(Appendix 1). Time or age of river systems is also going to be very important for future studies because it will provide

new information about the lateral migration rates of river systems and if the lateral migration rate is known then details about bank material and flow characteristics can be inferred (Howard and Knutson 1984). Looking at the channel courses (Figure 1A), where three channel courses of the same river represents three different points in time overlap one another and the total amalgamation creates the channel-belt (Figure 1B). The spacing of unconformable points is not only a way to study the time component of channel belt creation but when compared with radius of curvature estimates about the width of the channel belt can be estimated.

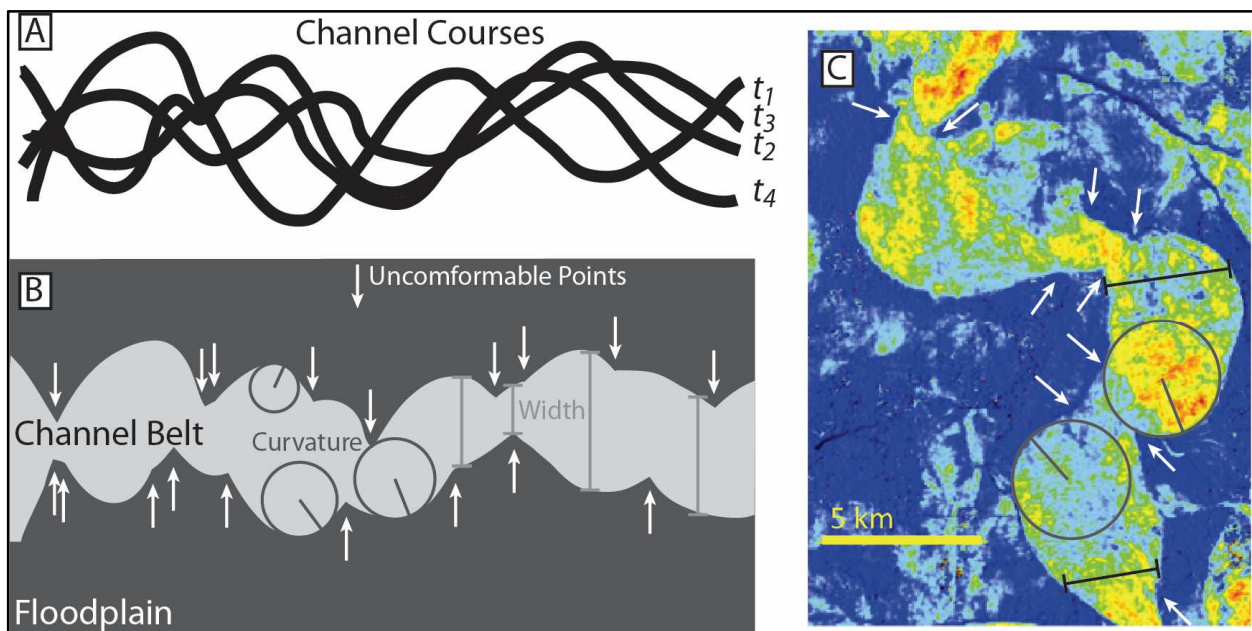


Figure 2: The Formation of a channel-belt. The four channel courses in (A) produce the channel-belt in (B). A) Shows the kinematic aspect of meandering channels, and how each previous channel course represents a different point in time. B) Illustrates the amalgamation of all previous channel courses to create the channel belt and how that translates being able to map the channel belt width, distance between unconformable points, and channel belt curvature. C) A Channel-Belt in late Miocene strata beneath the Mississippi Delta resolved in the warm colors of the sweetness attribute from a seismic volume (modified from Armstrong et al., 2014 prepared by J. Shaw).

The relationship between the channel belt morphologies is also important; it better illustrates the interaction between the modern channel and the channel belt. The relationship between ( $L$ ) and ( $P_{cb}$ ) can be used to calculate the angle arc of the meander preserved on the channel belt ( $\alpha$ ).

The ( $P_{CB}$ ) relationship with the ( $P_C$ ) provide information about how similar the characteristics of the modern channel is to the channel in the past.

## 1.4 Literature Review

### 1.4.1 Jefferson (1902)

Belt width has been studied before in multiple capacities. Jefferson (1902) studied meander belt dimensions in relation to the channel as well as the meander belt width in relation to the meander wavelength. This study is unique in that it is found cited in numerous other studies, yet there has been almost not follow research testing Jefferson's work. Jefferson measured fifty reaches of rivers in North America. The length of the studied reaches is not clear, but based on figures published in the study the reaches range from a few kilometers to roughly fifty kilometers (Figure 3). Which is significantly shorter than river reaches in this study, which ranges from forty river kilometers to three hundred fifty kilometers.

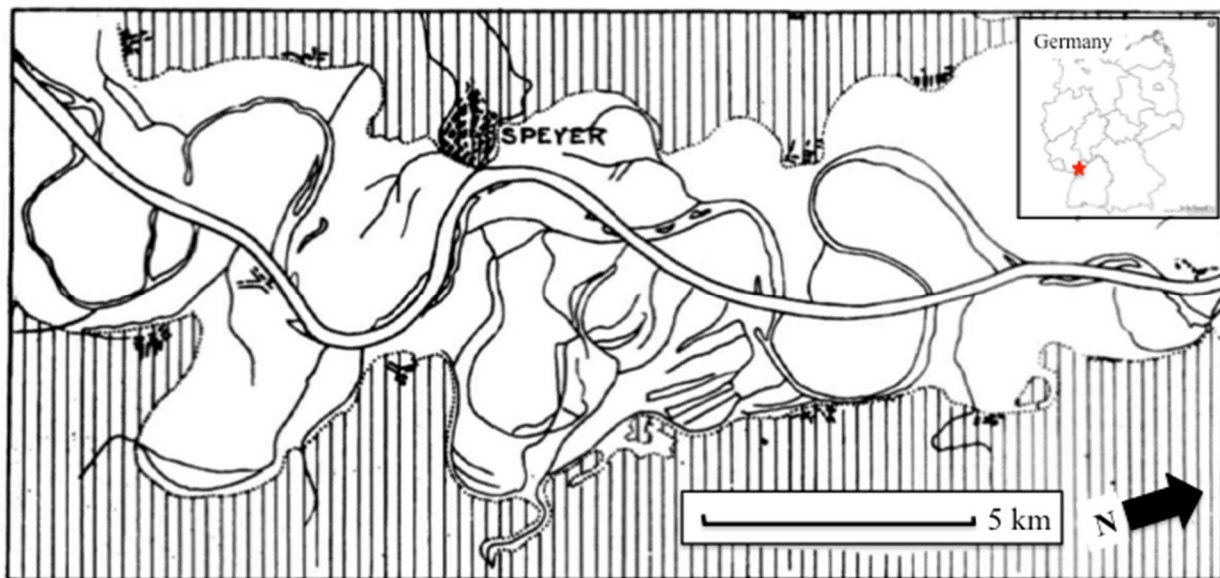


Figure 3: Map focuses on the Rhine River near Speyer, Germany. The un-shaded area around the river channel is representing the channel belt (Modified from Jefferson, 1902).

The method measuring belt width is similar to the one used in this study, where the width of the meander belt is measured perpendicular to the downstream direction. However, the meander

belt is not interchangeable with channel belt. The meander belt is the measure of the outermost outer bank width. This is a very common method for studying river systems, however, I believe that it leaves out a lot of channel morphology that is preserved on the surface. The meander belt width measurement is then divided by the mean channel width to create the variable, which can be seen in equation 1.

$$\frac{W_{MB}}{W_C} = W^* \quad (1)$$

Jefferson's (1902) study determined that a river's meander belt width is on average,  $W^* = 18$ . The  $W^*$  equation was adjusted for this study and will be discussed in Data Processing. While significant for the time, the study doesn't describe any of the variation within the data set or within individual rivers. Some rivers fluctuate between the minimum and maximum widths over the distance of the river reach, which is why the longer the length of the river reach measured the more accurate the representation will be of the entire river system. This study will quantify the variance in channel width as well as median statistics for the data set and individual river reaches. It will also create constraints for rivers not included in this data set but are similar to it.

#### **1.4.2 Leopold and Wolman (1960)**

A commonly cited study focusing on meandering river bends, titled River Meanders, develops a theory that proves a relationship between the meander radius of curvature and the river velocity and flow characteristics (Leopold and Wolman 1960). One reason this study is so heavily cited is because of the breadth of the research. The study looked at radius of curvature of the meander bends in relation to channel width, meander wavelength, cross-sections through meanders, flow patterns through meanders, meanders without sediment. The study addressed several problems with meandering rivers dynamics. The first problem is there are multiple mechanical and hydraulic processes that govern form, size, and occurrence of meanders. The

second problem is the physiographic history of a channel may have been destroyed by channel erosion after it was deposited. The channel belt morphology characteristics measured in this study are the meander wavelength, amplitude, and the mean radius of curvature. The study concluded the mean ratio of radius of curvature to meander width ranges from two to four, which coincides with other studies (Leopold and Wolman 1960; Hickin and Nanson 1984). The range found in those studies is perfectly acceptable, however, the method used only makes one radius of curvature measurement at the apex of the meander bend (Leopold and Wolman 1960; Williams 1986). The method used in my study makes multiple measurements per meander bend which provides a better understanding of the actual meander shape rather than general understanding.

It was also concluded that meander length, channel width, and radius of curvature are not determined by how erosive the channel banks are but rather some unknown mechanical process (Leopold and Wolman, 1960). This was significant because the amplitude was previously determined to increase moving downstream by the U.S. Waterways Experiment Station due to a correlative increase in the erosiveness of the channel banks (Friedkin, 1945). Their study discovered multiple interesting characteristics for meandering rivers, such as it being rare for rivers to straighten for longer than ten channel widths downstream (Wolman and Leopold, 1957), meander length is usually seven to ten times the channel width for that location, and the ratio of the mean radius of curvature is two to three times the channel width at that meander (Leopold and Wolman, 1960). The Leopold and Wolman (1960) methodology for radius of curvature differs from the methodology presented here, where other studies makes one radius of curvature measurement at the apex of the meander bend I have taken many to show a distribution of the entire meander bend.



### **1.4.3 Alford and Holmes (1985)**

Other studies focus on the planform geometry and migration, much like this study does, but rather than relating the channel-belt geometry with the channel these studies focuses on the planform geometry of specific ancient channels (Alford and Holmes (1985). Alford and Holmes (1985) showed that Pleistocene and Holocene climate changes near the Sabine River in Southwest Louisiana. This study focused on the meander wavelength and the radius of curvature of what they call ‘fossil-features’. These ‘fossil-features’ are simply abandoned river channels that are apparent in aerial imagery. These ‘Fossil-Features’ are not necessarily on the edges of the channel-belt such as in their study but were classified in to sixteen categories (Brice 1974). It was ultimately determined that because the channel belt morphology of interest in my study was tied to discharge and discharge was linked to paleoclimate, then the channel belt morphology could be linked to paleoclimate (Alford and Holmes 1985).

### **1.4.4 Gibling (2006)**

There has been a tremendous amount of research based on the study of meandering river systems in the stratigraphic record. These studies focus on the three-dimensional geometry of the river channel body deposits and scour fills (Gibling 2006). The motivation behind the Gibling (2006) study of fluvial channels width, thickness, and valley fills was due to the amount of research on the internal organization of channel bodies and comparative lack of research on the three-dimensional or external geometry of the channel bodies. The studies done by Martin (1993) and North (1996) investigate the channel body geometry by plotting the width of the channel bodies against the thickness of those bodies in logarithmic space; these are the types of studies data and methods were collected from for the Gibling (2006) study. By collecting data from other studies it allowed for the representation of 155 stratigraphic units. Gibling (2006) studied

the  $W/T$ , where  $W$  is width and  $T$  is thickness of the channel, for braided systems, meandering systems, fixed river systems, avulsion/crevasse splay deposits, floodplain channels, valley fills, etcetera. My study is most interested in the findings of meandering systems where the values are restricted to a discrete area on the chart (Gibling 2006). There is some overlap within the meandering systems with the braided systems. The thought behind this is attributed to the lateral migration of the meandering system deposits. This fluvial-body geometry can now be used in the classification of channel-deposits, in addition to the already well-studied geomorphic setting and internal organization. The meandering river systems are identified by their lateral accretion deposits are  $< 38$  m thick and  $< 15$  km wide. Gibling (2006) was studying the channel belt deposits in the stratigraphic record rather than a planform study of channel belts exposed on the Earth's surface, therefore, the Gibling (2006) study does not show where modern rivers, such as the Mississippi, can have channel belt widths exceeding 15 km.

## **2. Data Location**

### **2.1 Rivers**

This study will examine the channel belt geometry of fifteen different reaches of rivers from around the world. The purpose of including rivers all over the world is to insure variety within the data set. While there is significant variation in this data set there are many river system types that are left out of this study, such as tidal dominated meandering rivers, tropical meandering rivers. Thus, conclusions drawn from this study are expected to apply only to uni-directional rivers in temperate to arid environments with very low gradients.

In Table 1, all of the rivers in this dataset are listed by the river reach name with its plate number (if it came from the Saucier (1994) study), State, County or Parrish, latitude and longitude of the beginning and ending for the reach, length of river reach in river kilometers, and

the software used to measure the desired geometric features. The belt slope was calculated based on the elevation of the beginning and ending locations of the river reaches in this data set (Table 2). All elevations and latitudes and longitudes were established in Google Earth Pro. Google Earth Pro has a lateral accuracy of +/- 10 meters and has a vertical accuracy of +/- 30 meters. This accuracy should be viewed as a systematic error and should not significantly affect the computation of river or channel belt geometry.

River	State	County/Parrish	Reach (Km)	Latitude (Beg.)	Longitude (Beg.)	Latitude (End)	Longitude (End)	Method
Muddy Creek	WY	Carbon	40	41°17'37.83"N	107°41'34.26"W	41°28'21.28"N	107°42'7.07"W	Arc GIS
Yazoo P.8	MS	Tallahatchie	300	33°59'12.73"N	90°21'10.46"W	33° 0'41.50"N	90°21'20.92"W	Image J
George/Yazoo P.9	MS	Yazoo	224	33° 0'14.06"N	90°23'23.76"W	32°26'34.79"N	90°55'7.76"W	Image J
Black P.10	LA	Tensas/Catahoula	281	31°58'16.92"N	91°15'27.43"W	31° 0'14.47"N	91°51'52.02"W	Image J
Big Widow P.8	MS	Coahoma/Sunflower	350	33°59'11.65"N	90°33'50.93"W	33° 2'21.66"N	90°42'15.84"W	Image J
Bear Creek P.8	MS	Leflore/Tallahatchie	185	33°28'3.09"N	90°21'1.23"W	33° 0'21.95"N	90°26'58.37"W	Image J
Mississippi P.11	MS	West Feliciana	197	30°58'22.38"N	91°39'34.74"W	30°12'19.87"N	91° 6'2.51"W	Image J
White P.6	AR	Arkansas	185	35°39'32.79"N	91°29'57.58"W	35° 0'40.90"N	91°28'45.15"W	Image J
Neches	TX	Tyler/Jasper	132	30°47'37.65"N	94°10'9.41"W	30° 3'12.20"N	94° 1'43.54"W	Google Earth
Mississippi P.5	MS	Dyer	200	36° 0'25.06"N	89°42'43.94"W	37° 0'41.25"N	89° 9'58.89"W	Image J
White P. 7	AR	Arkansas/Bolivar	180	34°43'56.42"N	91°22'6.61"W	33°59'20.78"N	91° 9'25.28"W	Image J
Arkansas P.7	AR	Pulaski	142	34°44'52.99"N	92°14'56.95"W	33°58'54.76"N	91°23'28.08"W	Image J
Bayou Teche P.11	LA	Avoyelles	222	30°59'53.81"N	92° 3'3.16"W	30° 0'13.71"N	91°48'43.50"W	Image J
Selenga	RU	Buryatia	140	52° 9'25.67"N	109°30'55.59"E	51°53'18.80"N	107°50'38.40"E	Arc GIS
Red	LA	Bossier/Cadd	50	32°37'41.75"N	93°45'4.96"W	32°56'31.71"N	93°49'25.88"W	Google Earth

Table 1: Location of all rivers in data set, length of river reach (measured along the channel), beginning and ending latitudes and longitudes, elevation for both beginning and ending locations, and the method used to study river reach.

River	State	Straight Line Length (m)	Beg. Elevation (m)	End Elevation (m)	Slope
Muddy Creek	WY	19312	1977	2047	0.00363
Yazoo P.8	MS	107826	40	25	0.00014
George/Yazoo P.9	MS	69202	25	18	0.00011
Black P.10	LA	122310	22	13	0.00007
Big Widow P.8	MS	104607	46	28	0.00017
Bear Creek P.8	MS	51499	37	30	0.00012
Mississippi P.11	MS	99779	13	3	0.00010
White P.6	AR	72420	77	51	0.00035
Neches	TX	83686	15	0	0.00018
Mississippi P.5	MS	120701	71	90	0.00016
White P. 7	AR	85295	46	42	0.00005
Arkansas P.7	AR	117482	71	49	0.00019
Bayou Teche P.11	LA	112654	16	0	0.00014
Selenga	RU	119091	636	513	0.00103
Red	LA	35405	45	51	0.00016

Table 2: From left to right, the river reaches in this data set, the state they are located in, the straight line distance between the beginning and ending points in meters, the beginning and ending elevations in meters, and the belt slope between the beginning and ending locations.

## 2.2 Lower Mississippi River Valley

A large portion of the reaches of rivers in this study came from a study by Saucier in 1994 of the lower Mississippi river valley in North America. The plates used to collect data for the lower Mississippi valley can be seen in Figure 4 and where they are in relationship to one another. The name of the river reach associated with the number in Figure 4 is seen in Table 3. Channel belt geometries used in this study were taken from the maps and were investigated based on his interpretations. The interpretation for the (Saucier 1994) study includes a wide variety of methods. The basic mapping was done with aerial imagery of multiple vintages. The multiple vintages of imagery are helpful for showing differences in vegetation and moisture levels, the older images were helpful for showing the landscape prior to implementation of farming in the area (Saucier 1994). The Saucier study did include some borings and core from wells in addition to the aerial imagery, this was done from previous work and eighty percent of what was known

at the time was restricted to less than twenty percent of the study area, so the majority of the work done was from aerial imagery.

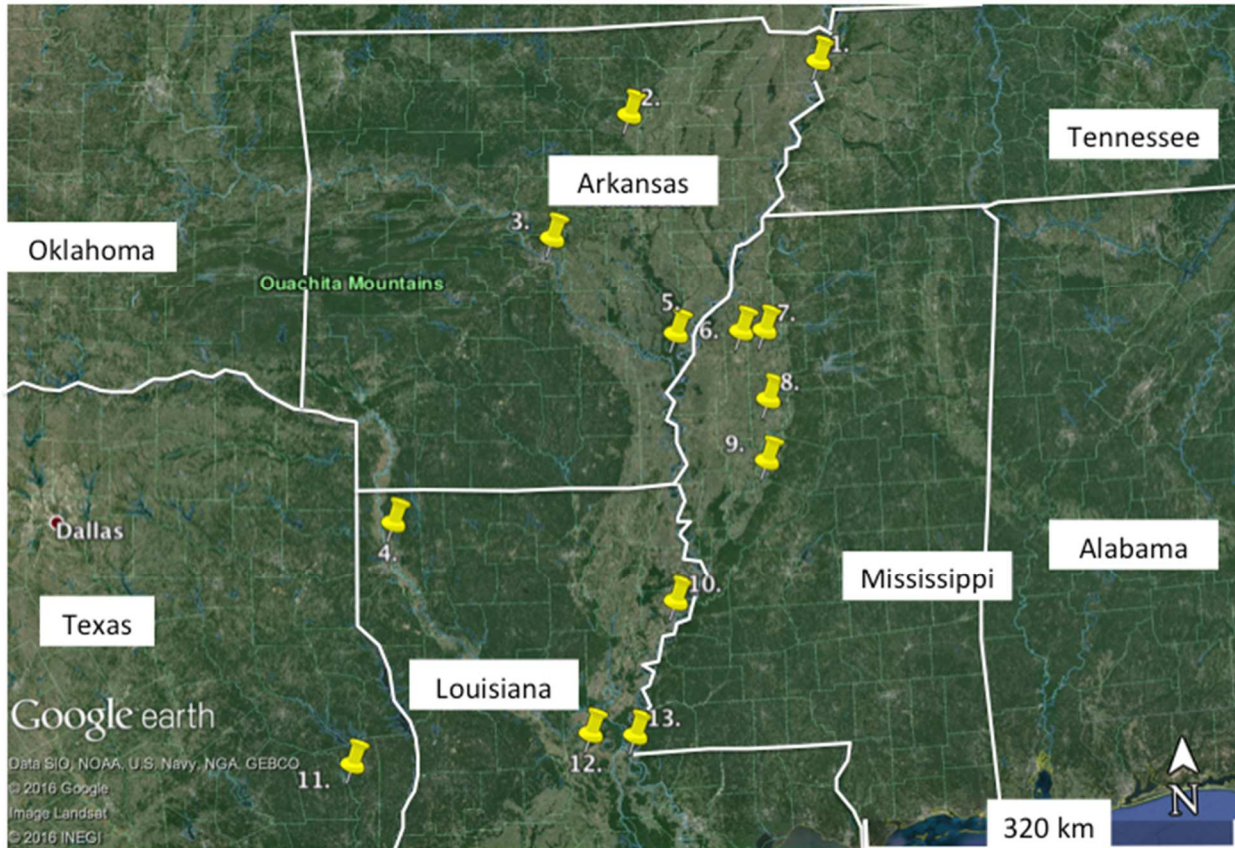


Figure 4: Illustration indicating relative location and reaches used in study. Number associated with map can be seen in Table 2. Modified from Google Earth Pro.

Number	Reach Name
1	Miss. Plate 5
2	White Plate 6
3	Arkansas Plate 7
4	Red
5	White Plate 7
6	Big Widow Plate 8
7	Yazoo Plate 8
8	Bear Creek Plate 8
9	George/Yazoo Plate 9
10	Black Plate 10
11	Neches
12	Bayou Teche Plate 11
13	Miss. Plate 11

Table 2: Numbered reaches found in Figure 4 associated with reach name.

### 2.3 Additional Rivers

Other rivers used in this study range are the Neches River in East Texas, the Muddy Creek in Southern Wyoming and the Selenga River in Southern Russia. These rivers were added because they add diversity to the data set while also producing an unambiguous channel belt. The Selenga River and Muddy Creek reaches are also incised valleys and are important to include because incised valleys often include desirable reservoir sediment as well as were included in previous studies of meandering river systems (Jefferson 1902; Martin et al. 2011).

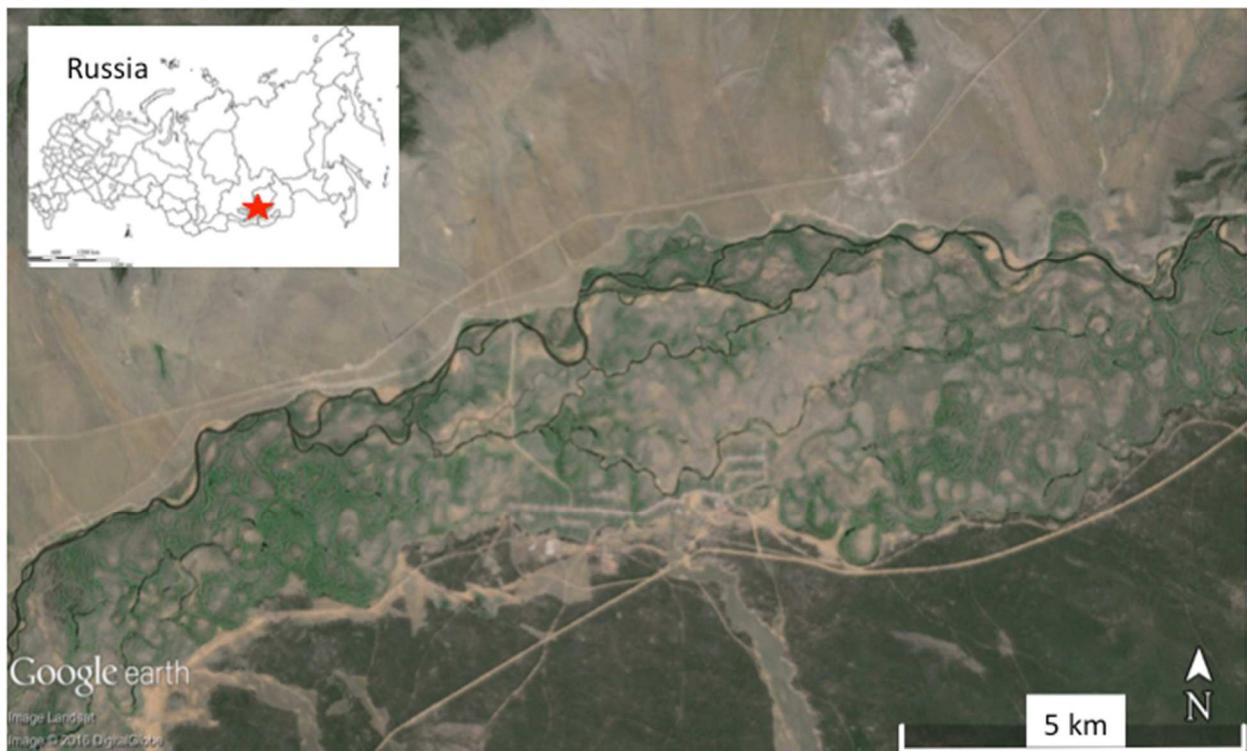


Figure 5: Image of the Selenga River in Buratia, Russia. This river system is an incised valley and is well preserved due to its desolate location. Modified from Google Earth Pro.

The Selenga River in Buratia, Russia, is an excellent meandering river system in a very rural area, so anthropologic impacts to the belt geometry are minimal (Figure 5). The 140 km river reach was chosen because that particular section of the river most visually illustrated the type of channel-belt this study was interested in. The Selenga is an incised river system. Nevertheless, it

the planform geometry of the incised valley exhibits similar varying belt width, meander scars and associated unconformable points to flood plain channel belts (Dong et al. 2016).

The reach of the Red River this study looked at began in Shreveport, Louisiana, and extends upstream for 50 km. There was some subjectivity in interpretations in some locations due to the farmland and other anthropologic influences; however, this reach of river is great example of the type of channel-belt this study is most focused on. The Neches River reach begins 132 km North of Beaumont, Texas. This river reach has an excellently preserved channel belt, however, it should be noted that it has been historically well documented that the river seen today is much smaller than it was in the past, particularly during glacial melting periods. This means that the river was much larger when it created the channel-belt seen today (Blum and Hattier-Womack 2009). Finally, there is the Muddy Creek reach found in Carbon County, Wyoming. This reach is excellent because of how clear the channel-belt can be seen in aerial imagery.

### **3. Methodology**

#### **3.1 Workflow**

This methodology was challenging to establish, however, the one I have developed is accurate and replicable (Figure 6). This study is measuring three different channel belt morphologies, the width of the channel-belt and channel, distance between unconformable points, and curvature of the channel-belt edges and channel. These features are to be normalized by the geometric mean of the river reaches respective channel width, then plotted in a cumulative distribution function with every other river in this data set.



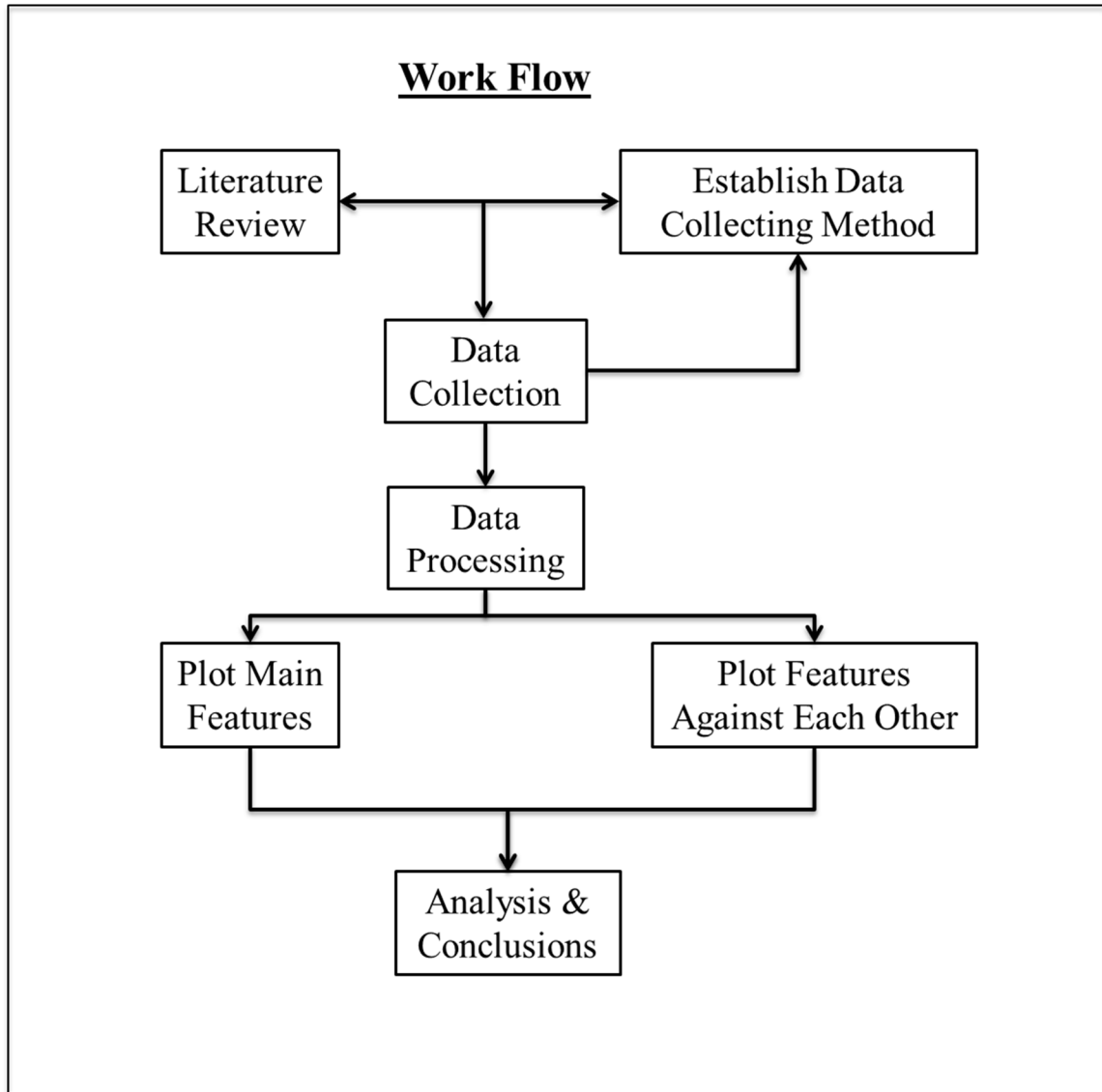


Figure 6: Workflow highlighting steps taken for completing study.

### 3.2 Software Selection

Finding the right software was crucial for the methodology for this study and within this data set there are three different forms of software were used to collect data (Table 1). ArcGIS works really well but when using free imagery from BING maps the resolution and ease of use is lacking compared to Google Earth Pro. Both of these software's work very well but it was found that ImageJ is the most intuitive, is open sourced, and requires you to have a scaled image so the internet was unnecessary to work properly.

### **3.3 Channel-Belt Identification**

The way channel belts are identified creates some subjectivity within this project. Many of the beautiful meandering rivers are in environments that could produce channel belts but are also in areas near major cities or farming communities. The ideal method for identifying channel belts lateral extent is by collecting actual samples of sediment to determine the furthest extent of lateral migration. Given the fact that this study has measured 2,828 river kilometers this method for channel belt identification was more than feasible. The second best method for channel-belt identification would be to use digital elevation model data where we would be able to identify changes in elevation. For the majority of the rivers in this study channel belt identification was done based on previous interpretations (Saucier 1994). For the reaches of rivers in this study that were measured based on the aerial imagery seen on Google Earth Pro and ArcGIS Bing Maps, channel belts were identified based on changes in the surface morphology interpreted to be produced by fluvial processes and changes in vegetation types (Figure 7). The erosional scars and depositional point bars created by previous flow paths of the river cause the channel belt morphology.

When measuring features in the Saucier data set channel belt identification was based on units labeled on plates. Plate 7 shown in Figure 8, shows Saucier's (1994) interpretation of the Lower Mississippi valley. The units for Figure 8 are indicated in Figure 9 by the Saucier (1994) legend. These deposits were labeled alluvial valley Holocene units on Saucier's (1994) maps. The deposits not used in identifying channel belts were alluvial fans, floodplain, and undifferentiated alluvium deposits. The abandoned channels are denoted by the yellow and blue. The light tan denotes various point bars. The Deposits labeled as deltaic and chenier plain Holocene deposits as well as Pleistocene deposits were not part of the identified channel belts.

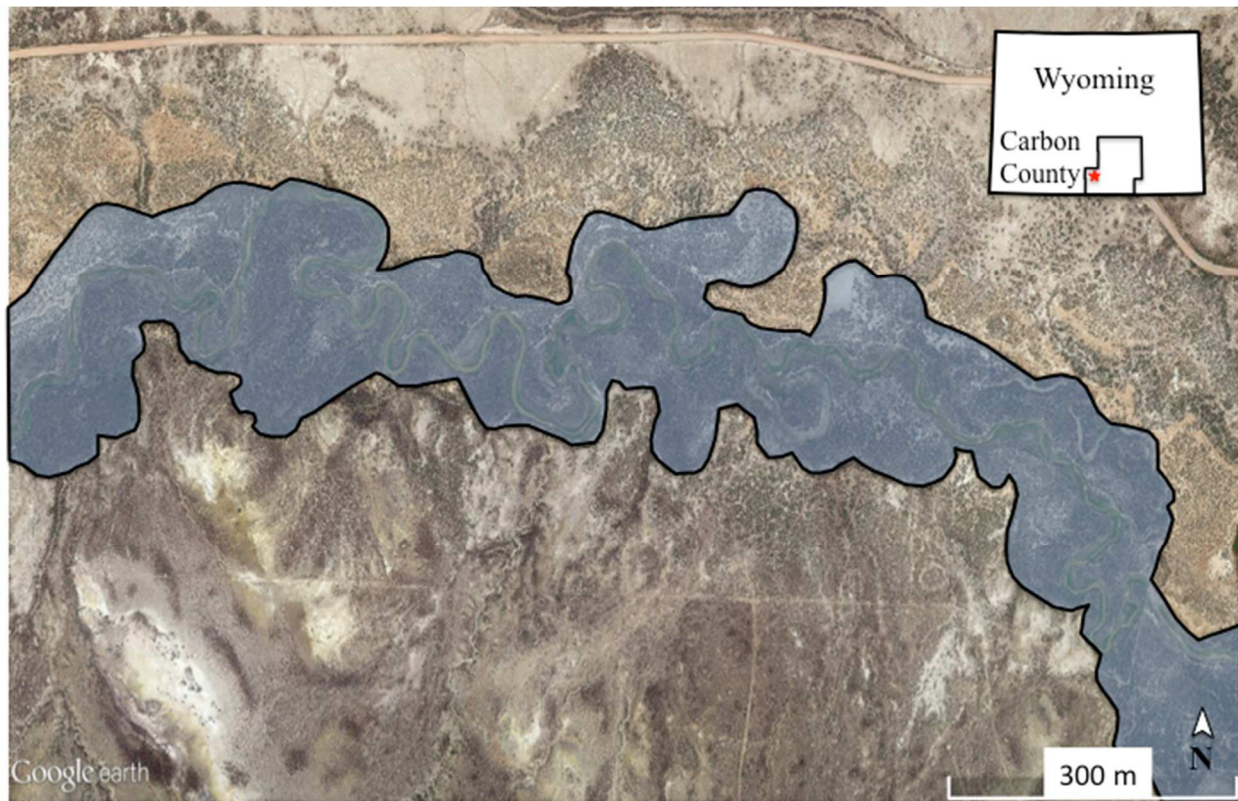


Figure 7: Portion of the Muddy Creek reach in Carbon, Wyoming. This image is showing the certain ambiguous features of distinguishing channel-belts in aerial imagery. Image taken from Google Earth Pro in 2016. The blue shaded area on the map is indicating what the channel-belt looks like in real life based on my interpretation. Modified from Google Earth Pro.

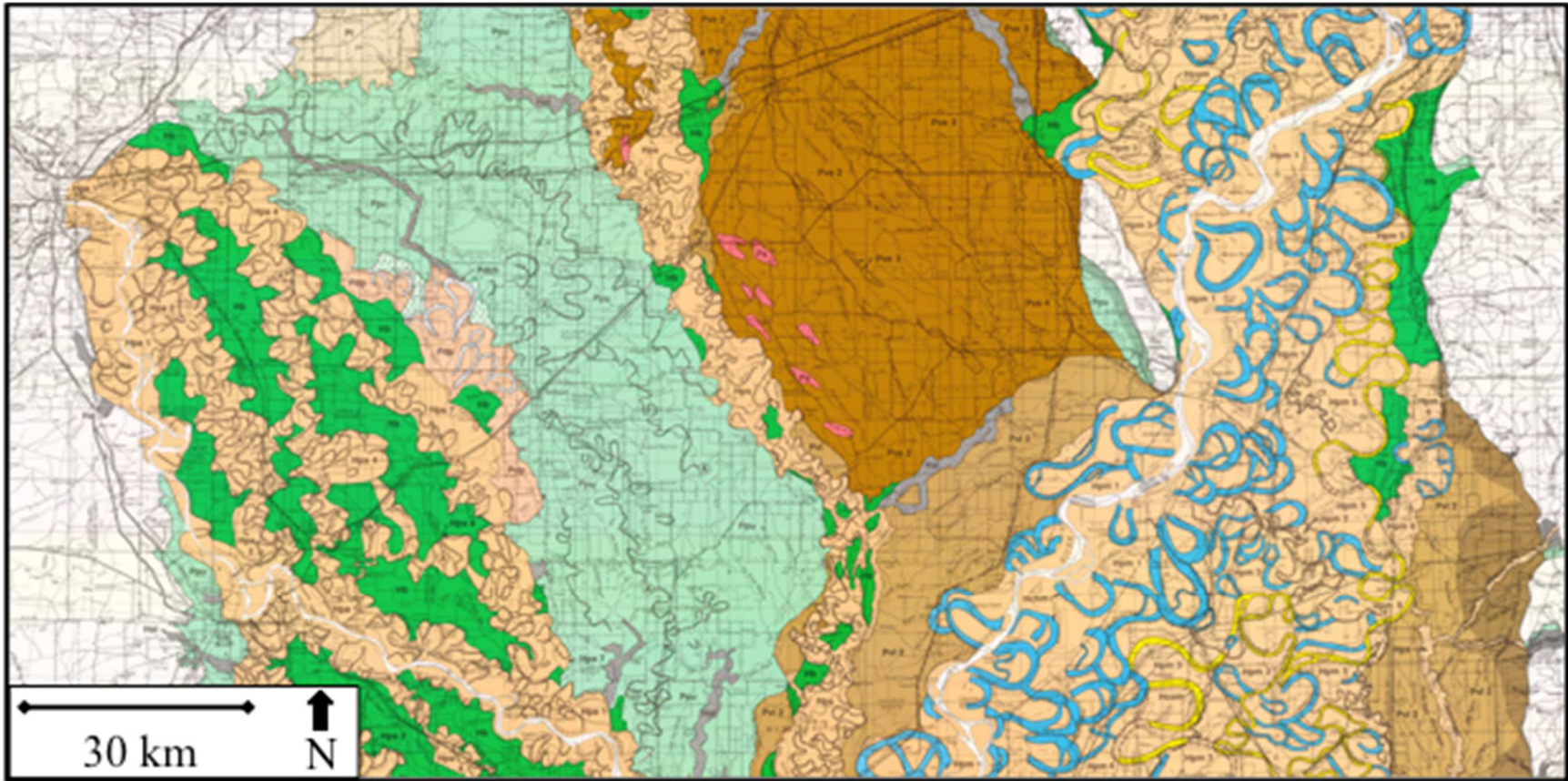


Figure 8: Plate 7 near Little Rock, AR, and is showing interpretations of all the units in the lower Mississippi valley. The light solid tan, blue, and yellow colors are indicative of the units that make up a channel-belt and thusly how I identified the channel-belt and measured them for this study (Saucier 1994).



## Holocene Units (Alluvial Valley)

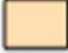


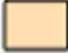
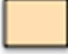
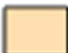
-  **(Hpm 1-6):** Point bar (meander scroll) deposits of Mississippi River meander belts 1 to 6 meander belts of different ages separated by hachured lines with tick marks on the older meander belt side.
-  **(Hchm):** Abandoned channels (neck and chute cutoffs) of the Mississippi River
-  **(Hcom):** Abandoned courses of the Mississippi River. Projected where removed by lateral migration of subsequent small streams. Includes trunk channels of the major delta complexes.
-  **(Hpa 1-8):** Point bar (meander scroll) deposits of Arkansas River meander belts.
-  **(Hpr 1-5):** Point bar (meander scroll) deposits of Red River meander belts 1 to 5.
-  **(Hps):** Point bar (meander scroll) deposits of small streams.

Figure 9: Legend showing colors indicating specific units used on plates and subsequently how channel-belts were identified for this study (modified from Saucier 1994).

### **3.4 Measuring Techniques**

The first step in channel belt measurement is to measure the channel belt width and channel width. Measurements are made in meters at the same time by using the straight line measuring tools found in ArcGIS, Google Earth, and ImageJ. Measurements are taken at approximately every river mile for the entire reach of river. The channel belt widths are made perpendicular to the channel belt orientation measured one channel belt width up and downstream from the location being measured. The channel width measurements are taken perpendicular to the flow path of the channel itself one channel width up and downstream from the point being measured, as shown in purple (Figure 10). The distance between unconformable points is also measured, in meters, using the straight-line measurement tools found in ArcGIS, Google Earth, and ImageJ (Figure 10).

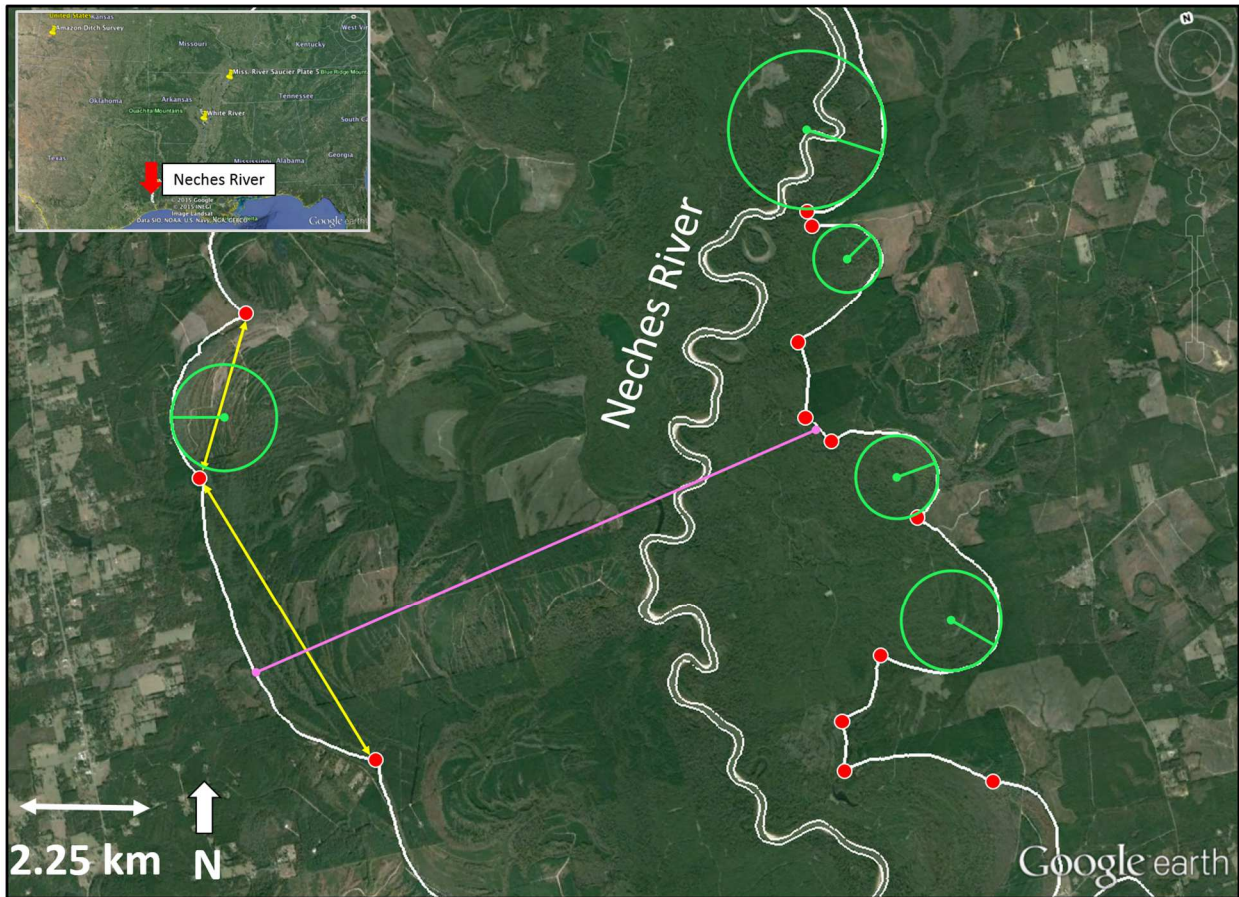


Figure 10: Neches River near Beaumont, Texas. The white outlines are showing the channel and channel belt paths. Examples of the radius of curvature (P) measurements along the channel belt can be seen in green. Examples of distance between unconformable points (L) can be seen in yellow with the actual unconformable points in red. Channel belt width (W) is seen in purple. Modified from Google Earth Pro.

Developing an efficient method for collecting radius of curvature measurements has been the most challenging issue in developing methodology for this study. The method finally settled upon is best performed in ImageJ but can be done in either ArcGIS or Google Earth. Using the multipoint tool in ImageJ several points are plotted and recorded at a density that allows for a minimum of twenty points per curve. In ImageJ these points will be plotted in X (Easting) and Y (Northing) coordinates which is preferred, however, in Google Earth and ArcGIS these points will be plotted in WGS 1984, Latitude and Longitude, coordinates. Next, they were converted to Easting and Northing coordinates based on their Universal Transverse Mercator zone. This is

done using Matlab, using the WGS2UTM1 coding for Matlab written by Alexandre Schimel at the University of Waikato in Hamilton, New Zealand.

### 3.5 Data Processing

Channel-belt widths, channel widths, and unconformable point spacing were measured manually and were entered directly in to Microsoft Excel. Data points collected for the radius of curvature were calculated in MatLab and exported to Microsoft Excel. Once all of the data was in Excel for the channel-belt width (m), channel width (m), unconformable point spacing (m), and radius of curvature (m) they were sorted, normalized and then the inclusive percentile function was applied.

The channel widths were used to help normalize the values from the channel-belt width, unconformable point spacing, and radius of curvature measurements. The way the channel width measured values help in the normalization process is by calculating the geometric mean of all of the channel width measurements for that particular reach of river. The geometric mean focuses on the tendency of values in a set by using the product of the values in the series rather than the sum, like seen in arithmetic means. The geometric mean is the  $n^{th}$  root of the product of  $n$  values. The geometric mean is a preferable statistic compared to the more common arithmetic mean when values range by orders of magnitude, as they do here.

Before anything was done with the channel-belt width (m) measurements they were normalized by the geometric mean of the channel width of the respective reach of river.

$$\frac{W_{CB}}{W_{MC}} = W^* \quad (1)$$

Where  $W^*$  is the dimensionless normalized value of the channel belt,  $W_{CB}$  is the width of the channel belt,  $W_{MC}$  is the geometric mean of the respective reach's channel width. Once this has been done the new  $W^*$  values were sorted from smallest to largest and then the inclusive



percentile function was applied. This was done so the three features measured can be compared at specific percentiles and so that the fraction of measurement below certain percentiles can be determined for the three features.

Much like the channel-belt width measurements, the spacing between unconformable points (m) needed to be normalized by the geometric mean of the respective channel width, which was done with equation 2.

$$\frac{L}{W_{MC}} = L^* \quad (2)$$

Where  $L^*$  is the new dimensionless normalized spacing between unconformable points,  $L$  is the spacing of unconformable points, in meters, between unconformable points, and  $W_{MC}$  is the geometric mean channel width for the respective channel.

The method established for this measuring the radius of curvature involved using a multi-point tool to mark points all along the edges of the channel-belt as well as the centerline of the modern channel. These point densities had to be tight enough in order to provide the most realistic image of the curve, typically, this meant a minimum of ten points per curve. This was done with the multi-point tool because the MatLab code used calculates the radius of curvature based on three points.

Before the radius of curvature can be calculated the points collected in ArcGIS and Google Earth Pro need to be converted from WGS 84 to UTM coordinates. The MatLab code used for calculating radius of curvature needs input points to be in Easting and Northing (X, Y) coordinates. The points collected via ImageJ are already in (X, Y) coordinates. To convert from WGS 84 to UTM coordinates the Matlab code, `wgs2utm1.m`, by Alexandre Schimel at the University of Waikato, was used. It was relatively simple, WGS 84 coordinates are input and UTM coordinates are output. Once the data points are in Easting and Northing coordinates they

need to be sub sampled so that super sampling doesn't occur. When super sampling occurs the values of the radius of curvature are extremely large indicated straight lines when that is not indicative of the actual channel-belt shape. Creating new points in Matlab at every geometric mean channel width downstream does the sub-sampling. Once the sub-sampling is done the data points can finally be used to calculate the radius of curvature by inputting them into MatLab code, Courbure.m code (Peyret 2011). This code works by taking the first three points of one edge of the channel-belt and calculates the radius of curvature, and then it repeats the process by moving one point down for the entire length of the reach. This allows the radius of curvature to be calculated at every point on the channel-belt rather than at every third point. Once this has been done the radius of curvature values can then be placed in to Excel where they can be normalized and sorted for plotted.

Once in Excel the radius of curvature values measured in meters are divided by the geometric mean channel width of the respective river reach as seen by equation three.

$$\frac{P_{CB}}{W_{MC}} = P_{CB}^* \quad (3)$$

Where  $P^*$  is the dimensionless normalized radius of curvature,  $P_{CB}$  is the radius of curvature along the channel-belt and is measured in meters, and  $W_{MC}$  is the geometric mean width of the channel of that reach. This same equation is used for calculating the  $P^*$  of the modern channel the only difference is  $P_{CB}$  is substituted with  $P_C$ , the radius of curvature, in meters, of the modern channel. After the  $P^*$  values have been calculated and sorted from smallest to largest, they are input in to the inclusive percentile function found in Excel that all the other features were input into.

The relationship between the spacing of unconformable points and the radius of curvature on the channel belt is showing the distribution relationship between unconformable points and the

radius of curvature on the channel-belt. Since small  $L$  values are not always in the same location as small  $P$  values, the fiftieth percentile is the going to be the most accurate representation of what can actually be found on the channel-belt. It was initially hypothesized that the relationship between these two features would be something greater than a 1:1 relationship because if no part of a bend from one path were overlapping another path the distance between the unconformable points would be twice that of the radius of curvature. In reality the hypothetical relationship of  $L$  and  $P$  if the meander was both a semi-circle and not cut off by later flow paths (Figure 11). What the data shows, however, are twelve of the fifteen river reaches being a 1:1 relationship or less. If the relationship between  $L_{CB}$  and  $P_{CB}$  is 1:1 that means  $L_{CB}$  is the same length as the radius of curvature:  $P_{CB}$ . This leads to the idea that the meander angle arc can be calculated and plotted as well (Figure 11).

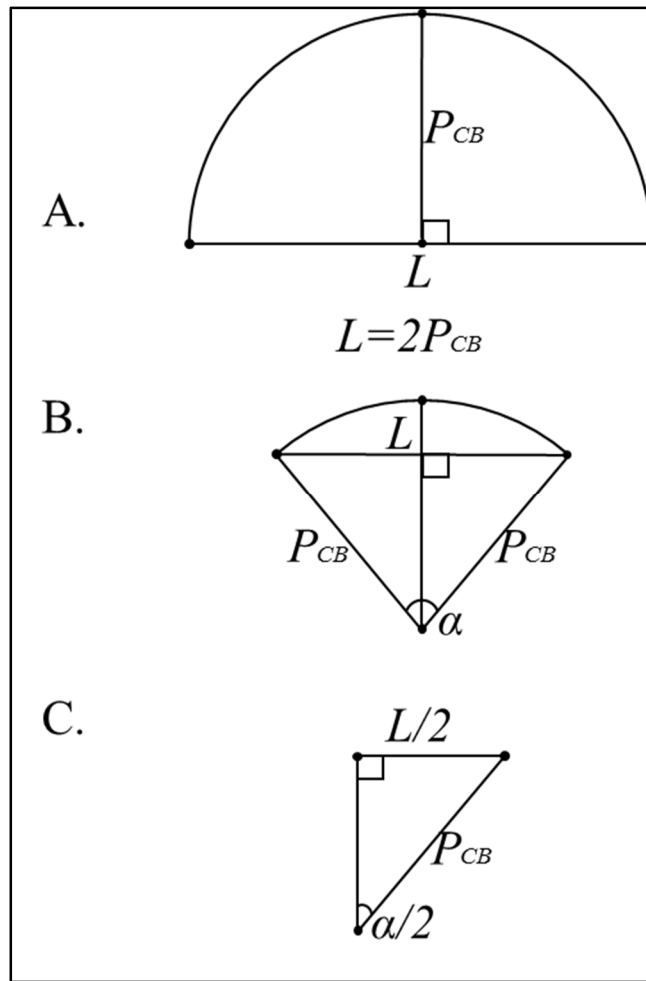


Figure 11: Calculation of preserved meander arc angle. A. Illustrating what the relationship between  $L$  and  $P_{CB}$  would look like in the hypothetical scenario where meander bend preserved on the channel-belt is a perfect semicircle and is uninterrupted by later flow paths. B. Illustrating a more realistic hypothetical scenario where  $P_{CB}$  creates a triangle for which and alpha is the meander arc angle. C. The triangle used to calculate angle alpha.

Upon calculating  $L/P_{CB}$  values for the 50<sup>th</sup> percentile each river reach and contemplating what that chart was showing, it was theorized that if a meander scar on the channel belt was not cut off by previous flow paths the shape left visible would be a perfect semi-circle and thus the  $P_{CB}^*$  values would be exactly half that of the  $L^*$  values. However, upon inspection of the  $L/P_{CB}$  values this is not the case because the kinematics of the river loops of random parts of the curve over time. If perfect semi-circles meander bends were preserved on the channel-belt  $L$  values would be twice that of  $P_{CB}$  values, (Figure 9). However, given that we only have a portion of the

semi-circle the  $P_{CB}$  value can make a triangle with  $L/2$ . From there basic trigonometry allows for the calculation of the angle of the arc left preserved on the channel belt,  $\alpha$ , in degrees. This can be seen in equation 4 and 5.

$$\sin \frac{\alpha}{2} = L/2P_{CB} \quad (4)$$

$$\alpha = 2\sin^{-1}\left(\frac{L}{P_{CB}}\right) \quad (5)$$

#### 4. Results

##### 4.1 Channel-Belt Width ( $W^*$ )

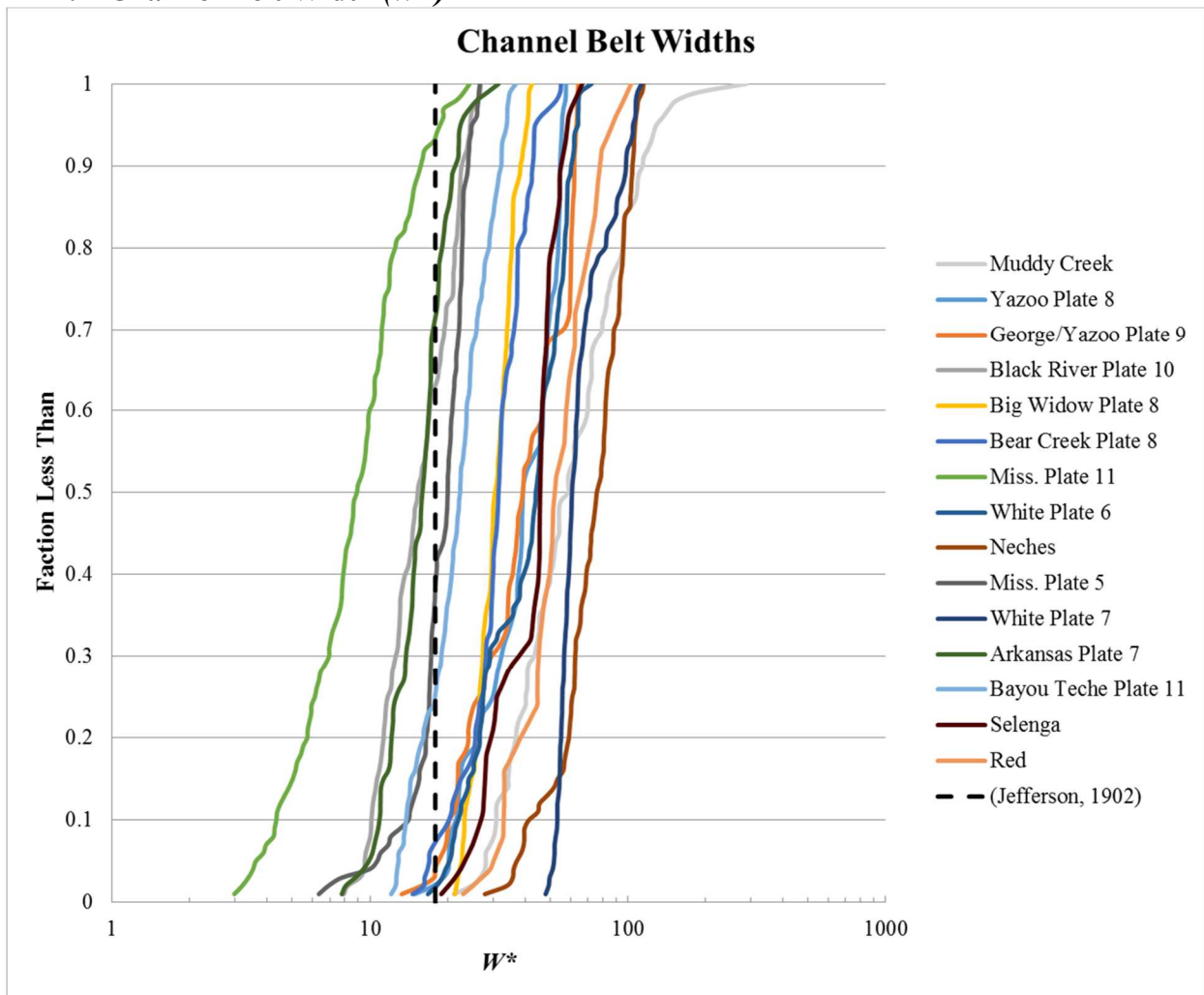


Figure 12: Chart is showing the percentile distribution of channel belt widths normalized by the geometric mean of the channel width.

The median variability of  $W^*$  for the river reaches in this data set start at 8.9 for the Mississippi River Plate 11 and ends at 76 for the Neches River (Figure 12). The variability in the

$W^*$  values at the tenth percentile begins at the minimum, 4.3, for the Mississippi River Plate 11 and a maximum of 53 for the reach White Plate 7. The variability at the ninetieth percentile starts with the Mississippi River Plate 11 at 16 and goes to the Muddy Creek reach with a value of  $1 \times 10^{+2}$ . While this range certainly includes the mean  $W^*$  calculated in the Jefferson (1902) paper, shown by the black dashed line, these new constraints between rivers show more variation than total mean shows (Figure 12).

While visibly it may appear like some river reaches are outliers from the data set, upon investigating the log rhythmic mean for the  $P_{50}$  values of  $W^*$ , it was found that no river reach within the dataset exceeded three standard deviations. This investigation was done for  $L^*$  and  $P^*$  also and no statistical outlier was found within the data set.

## 4.2 Spacing of Unconformable Points ( $L^*$ )

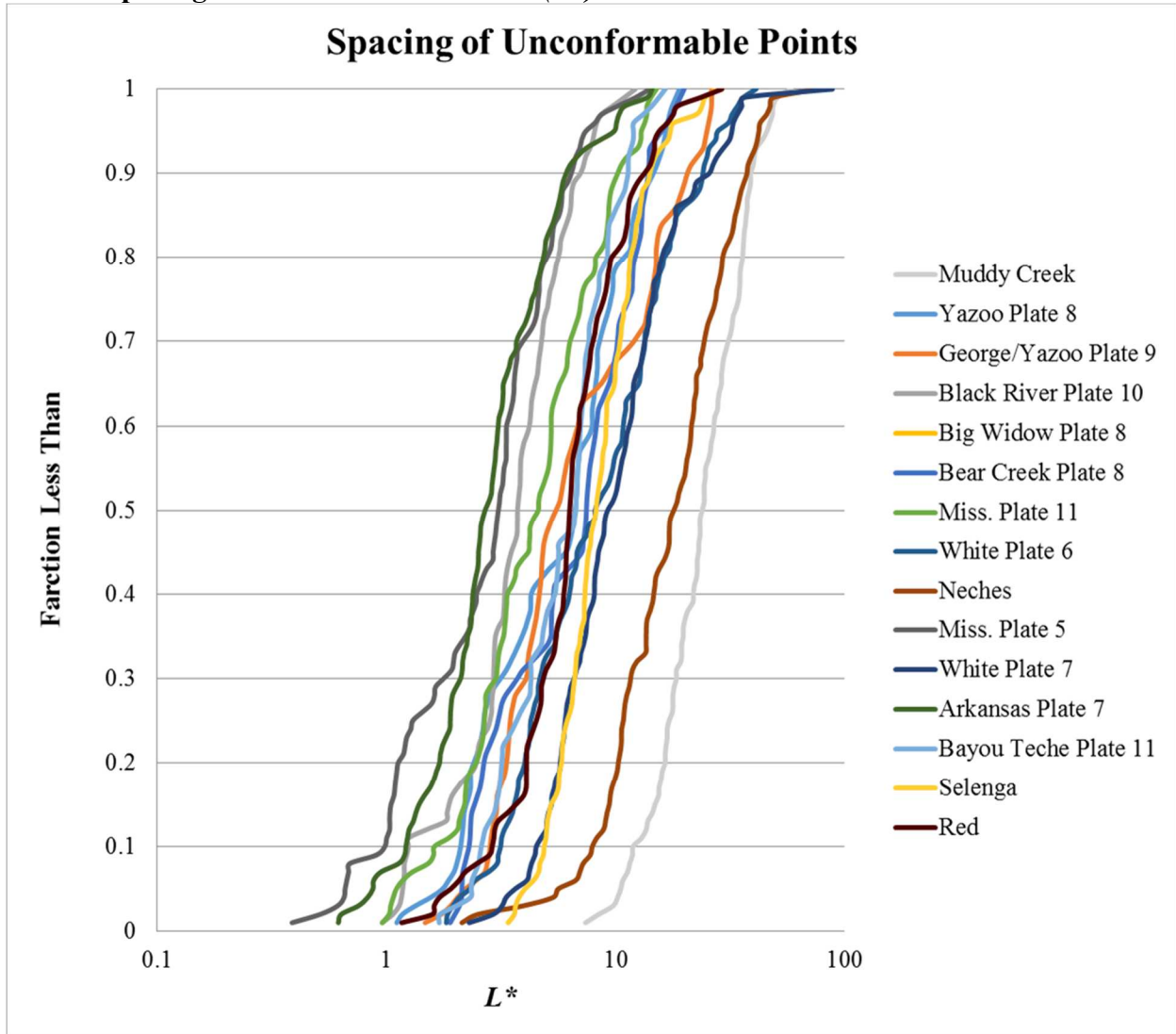


Figure 13: Shows the percentile distribution of the distances between unconformable points normalized by the geometric mean of the channel belt. This measurement has some subjectivity to it due to the fact that not all unconformable points can be seen when plotted against other measurements this subjectivity should go away.

Spacing of unconformable points is a metric, which provides clear variation constraint on the channel belt. The variation with  $L^*$  seen within the data set shows the spacing of unconformable points being roughly 1 to 10 times as large as the geometric mean channel width (Figure 13). The median range of  $L^*$  is 2.7 to 24 for the data set. The variability in the  $L^*$  values at the tenth percentile for all river reaches start with the Mississippi Plate 5 at 0.98 and have a maximum of

12 for the Muddy Creek. For the ninetieth percentile the minimum  $L^*$  begins with the Arkansas reach at 6.1 and has a maximum of 37 on the Muddy Creek reach.

### 4.3 Radius of Curvature ( $P_{CB}^*$ )

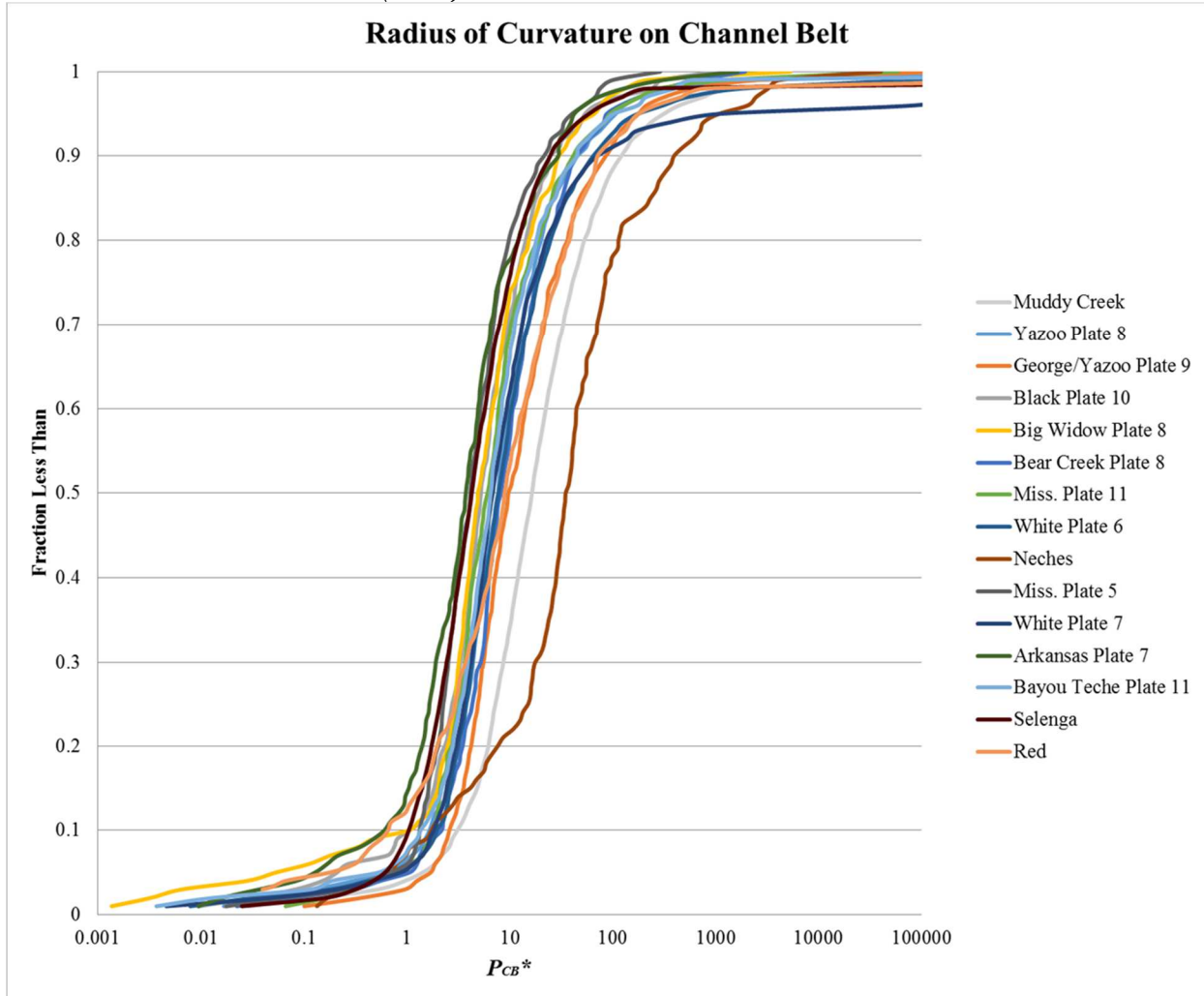


Figure 14: Percentile distribution of the radius of curvature of the channel belt normalized by the geometric mean of the channel.

The distribution of  $P^*$  for all rivers in the data set shows that the radius of curvature for the majority of the data set is 1 to 100 times larger than the geometric mean channel width (Figure 14). The median range for  $P^*$  within the data set begins at 3.8 and goes to 35. The tenth percentile minimum value for  $P^*$  is 0.6 on the Arkansas reach and has a maximum of 3.1 on the



Muddy Creek reach. The ninetieth percentile has a minimum value of 25 for the Selenga reach and has a maximum of 395 for the Neches River reach.

#### 4.4 P<sub>90</sub>/P<sub>10</sub>

Variation within the data set and within the river reaches is something that has been of large importance in this study. The statistical variation within the data sets is something that was left out of previous studies. In effort to rectify this, I calculated the P<sub>90</sub>/P<sub>10</sub> values for every river reach's  $W^*$ ,  $L^*$ , and  $P_{CB}^*$  data (Table 3). This statistical measure shows variation within individual rivers there is quantifiably less variation within individual river systems than in between rivers. The P<sub>90</sub>/P<sub>10</sub> values seen in this data set for  $W^*$  is less than 4, for  $L^*$  less than 8, and for  $P_{CB}^*$  generally less than 50.

<b>River</b>	<b><math>W^*</math> P<sub>90</sub>/P<sub>10</sub></b>	<b><math>L^*</math> P<sub>90</sub>/P<sub>10</sub></b>	<b><math>P^*</math> P<sub>90</sub>/P<sub>10</sub></b>
Muddy Creek	3.7	3.3	39
Yazoo P.8	2.5	6.9	27
George/Yazoo P.9	3.1	7.2	33
Black P.10	2.2	5.6	23
Big Widow P.8	1.6	5.5	28
Bear Creek P.8	2.1	6.1	20
Mississippi P.11	3.6	6.3	22
White P.6	2.7	7.6	33
Neches	2.5	4.7	227
Mississippi P.5	1.7	6.5	16
White P. 7	1.8	5.7	39
Arkansas P.7	2.0	5.0	49
Bayou Teche P.11	2.3	4.4	33
Selenga	2.0	2.9	24
Red	2.4	4.6	108

Table 3: P<sub>90</sub>/P<sub>10</sub> values calculated for  $W^*$ ,  $L^*$ , and  $P_{CB}^*$  for all rivers in the data set

#### 4.5 Radius of Curvature (Channel Belt vs. Channel)

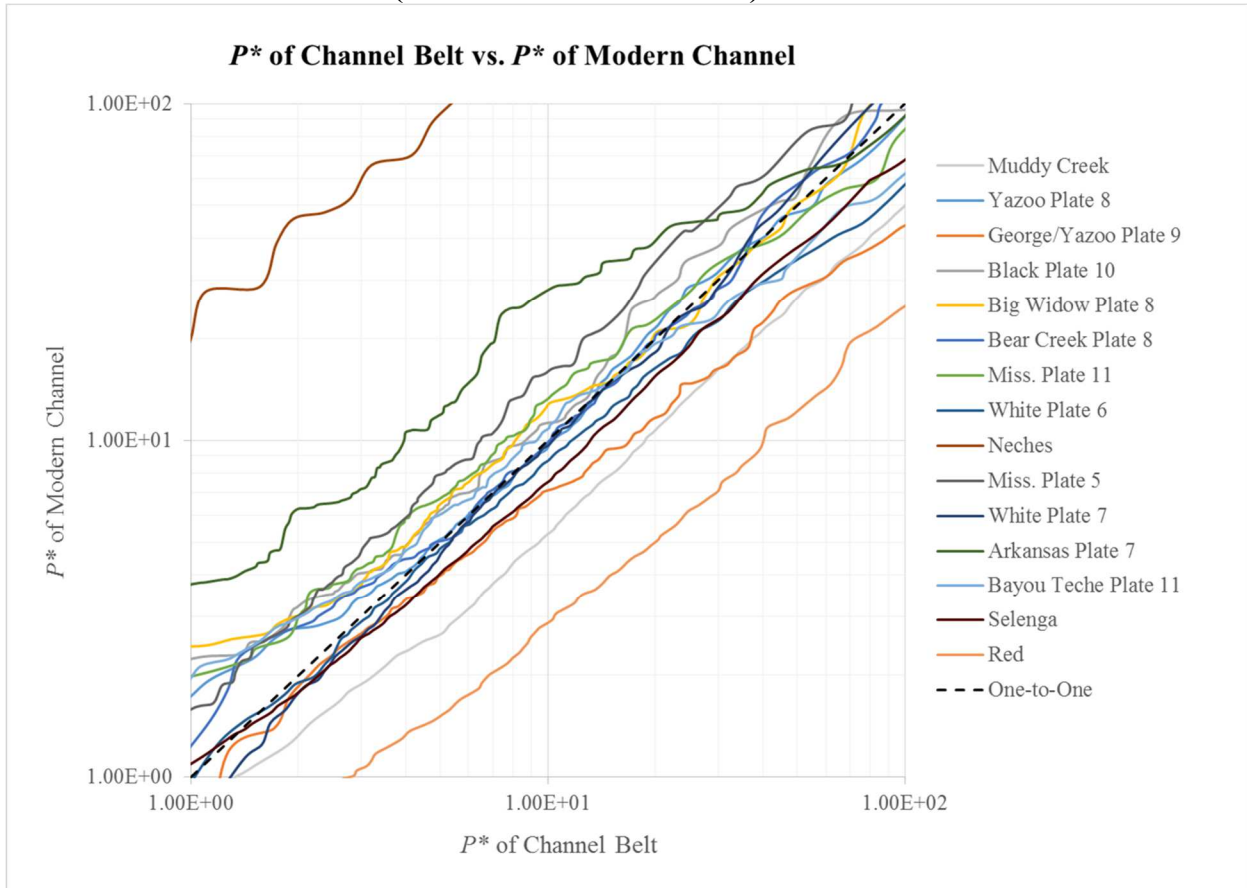


Figure 12: This chart is illustrating the relationship between the river reaches channel-belt and their respective channel. The  $P^*_{CB}$  values are divided by the  $P^*_C$  values and the new  $P$  value is plotted in a cumulative distribution plot.

Radius of curvature of the channel belt plotted against the radius of curvature of the modern channel shows how closely correlated the two measurements are for the data set (Figure 12). The statistical relationship is very close to one to one, which indicates the variables that make up the modern channel are equivalent to the variables of the channel in the past that made up the channel belt. There is the visible outlier of the Neches River but it has already been discussed that it is well known that the channel-belt was created by the evolution a much larger river than the modern channel due to previous glacial melting.

#### 4.6 Relationships Between Channel Belt Morphology

It was originally thought that all of the channel belt morphology measured in this study would be able to be plotted in relation to each other in a cumulative distribution function. However, once data was calculated and sorted to plot it became unlikely for measurements of different channel belt morphologies to related to the same location of the river reach and given that variability within a river has been established, the only calculations that could be reasonably used were the median values of  $W^*$ ,  $L^*$ , and  $P_{CB}^*$ . This is still useful in determining the relationship between certain features and creates variability ranges for those relationships for meandering river systems that create channel-belts.

The values calculated can be seen in Table 4, the three features that were measured for this study were directly compared to each other. The  $W^*$  median values were divided by the median  $P_{CB}^*$  values. The median  $L^*$  values were divide by the respective  $P_{CB}^*$  values. And the median  $W^*$  values were divided by the median  $L^*$  values. Since  $W^*$ ,  $L^*$ , and  $P^*$  values were dimensionless once they are divided they remain dimensionless.

For  $W/P_{CB}$  the range started at 1.4 for the Mississippi River Plate 11 and extends to a maximum of 10 on the Selenga River. For  $L/P_{CB}$  the minimum started with the Neches River at 0.51 and has a maximum of 1.9 on the Selenga River. With a maximum value of almost two that is indicating that  $L^*$  values are almost twice as large as the  $P_{CB}^*$  values. Based on the theory in this paper about how much of a meander bend is preserved in the channel-belt, the Selenga River's average is preserving almost the entire semi-circle and the Neches River is eliminating about 75 percent of the semi-circle. Both of these rivers are on the extremes though with many of the other rivers being closer to a one to one relationship. The  $W/L$  relationship starts with the Mississippi on Plate 11 with a value of 2.0 and goes to the Red River, which has a value of 8.3.

Angle alpha ( $\alpha$ ) is something that revealed itself in the data processing. Angle alpha ( $\alpha$ ) is the preserved meander angle arc on the channel belt. The median range of  $\alpha$  for the data set starts with a minimum of 29° for the Neches River and goes to a maximum of 148° for the Selenga River (Table 4). It would be ideal to calculate this for many locations on the channel belt however this study did not lend itself to such calculations at this time. However, this is significant because it means roughly a different flow path cuts half of the meander bend off.

<b>River</b>	<b><math>W/P_{CB}</math> Med.</b>	<b><math>L/P_{CB}</math> Med.</b>	<b><math>W/L</math> Med.</b>	<b><math>\alpha</math> (degrees) Med.</b>
Muddy Creek	3.43	1.44	2.49	92.8
Yazoo P.8	5.21	0.75	6.17	51.2
George/Yazoo P.9	3.79	0.56	6.94	32.8
Black P.10	2.89	0.70	4.14	41.6
Big Widow P.8	6.02	0.91	6.19	59.5
Bear Creek P.8	3.74	0.75	4.22	53.7
Mississippi P.11	1.43	0.73	1.97	44.1
White P.6	5.52	1.05	5.28	62.8
Neches	2.06	0.50	4.17	29.7
Mississippi P.5	4.74	0.63	6.43	43.5
White P. 7	8.69	1.36	6.28	84.8
Arkansas P.7	4.19	0.72	5.75	42.1
Bayou Teche P.11	3.34	0.99	3.39	61.7
Selenga	10.4	1.88	5.13	148
Red	5.58	0.68	8.32	41.4

Table 4: The median values for the calculations of  $W/P_{CB}$ ,  $L/P_{CB}$ ,  $W/L$ , and  $\alpha$ . (Med. = Median)

## 5. Discussion

### 5.1 Channel Belt Width

The median range of  $W^*$ , in my study, includes the mean of 18 from the Jefferson (1902) study but is quite a wide range when compared to that mean. There are a couple reasons a difference between this studies  $W^*$  values and those values of (Jefferson 1902) might be as large as it is. The first is a difference in the number of reaches of rivers between the two data sets. The Jefferson (1902) study contained fifty river reaches and this study only included fifteen reaches.

The second difference, and arguably the more important reason for explaining the difference between the two studies, is the two different methodologies. The Jefferson (1902) paper is not abundantly clear about the methods used as far as the spacing between measurement points, how the channel belt was identified, or the length of each river reach. These are important pieces of information to know about the data set. Judging by the figures in the Jefferson (1902) paper the length of the river reaches that were used were around 80 kilometers or shorter, where as in this study, the river reaches was 40 kilometers or larger, the largest being 300 plus kilometers. This study likely was able to capture a more accurate representation of the whole river system rather than just a portion of the river. The Jefferson (1902) paper does not disclose how the channel-belts were identified; it is entirely possible that given the maps that he was using were not detailed enough to identify the channel belt accurately.

Something else absent in Jefferson's (1902) paper is any kind of statistical measure that shows the amount of variation between the highest values and the lowest. This is crucial because as evident by the distribution plot there is not only tremendous variation between the different river reaches but there is also a tremendous amount of variation within a single river reach. The dataset presented here shows the median range for the data set is 8.9 to 76. This may not have been as important in this study if they were only focusing on particular points within the river, however, when looking at the distribution of measurements along a reach of river it is very valuable knowledge to know the amount of variation within the calculations that are being made.

## **5.2 Spacing of Unconformable Points**

The measurement and statistical analysis of this feature is completely new to the science and based on findings in this study is going to be a promising feature to help scientist better understand the percentage of meanders that are preserved and how much is removed by more

recent flow paths. Although I originally expected that the spacing between these unconformable points could lead to understand age constraints of the river system this is no longer the case. In theory the older the river system the more unconformable points it should have, however, whenever the system experiences larger migrations of the channel it is likely to remove multiple unconformable points at once.

The variation within the  $L^*$  shows the distance between unconformable points is never less than the geometric mean channel width. This seems somewhat intuitive due to the fact if part of the modern river channel is flowing on the edge of the channel belt it can only meander back towards the middle of the channel-belt so sharply and the width of the river is going to play a huge role in how sharp that meander can bend.

The spacing of the unconformable points on the channel-belt is the feature that has been unstudied until now. It is thought, though, this will become a noteworthy feature to study for multiple reasons. The lateral migration kinematics of river channels is difficult to distinguish in outcrops, thanks to the many features a river channel can produce and then stack on top of one another. Because of this stratigraphers have tried their best to study and comprehend what they can see but if there was a way to help model rivers by understanding their kinematics and thus how the channel-belt is evolves it would a tremendous accomplishment.

### **5.3 Radius of Curvature of Channel Belts and Channels**

As stated before the radius of curvature is something that has been studied before but not by taking the distribution of the edge of the channel belt. The data in this study shows a very good correlation between all of the river reaches (Figure 11). This is good for multiple reasons, the first being that most studies examine the radius of curvature for specific meander bends. In contrast, this study includes the entire distribution of radius of curvature measured at equal

intervals for the length of the river reach. For this dataset the radius of curvature was calculated in the tight meander bends as well as the portion of the river that are straighter. This study also calculated the radius of curvature for multiple locations within a meander bend rather than one measurement per meander bend. Both the incorporation of measurements outside of the meander bend as well as multiple measurements within the bend is likely what causes the correlation to be so strong within the entire data set.

It is also important that the curve trend very close to vertical and this correlation holds true for close to eighty percent of the river reaches and the correlation is strong throughout the distribution. This is significant because it shows there is not only a relationship between the modern channel of a river and its channel-belt, it seems there is a virtual direct relationship between the two. This will be useful when examining rivers where the most recent channel can be measured and compared with measurements taken from the channel-belt because it will quickly become clear if the most recent channel was comparable in size and flow characteristics to the older flow paths that created the channel-belt.

#### **5.4 Angle $\alpha$**

The calculation of angle  $\alpha$ , the preserved meander arc angle, is significant for understanding the morphology of meandering rivers and the petroleum reservoirs they create. The size of angle  $\alpha$  is directly related to the ratio  $L_{50}/P_{50}$ . Whenever the ratio  $L_{50}/P_{50}$  is large, angle  $\alpha$  is also large. Conversely, whenever the ratio  $L_{50}/P_{50}$  is small, angle  $\alpha$  is also small.

The variation of angle  $\alpha$  is rather large, ranging from 30° to 148°. I hypothesize that this range is attributed to the relationship between the lateral migration rate and the age of the river system. This relationship would mean that whenever the lateral migration rate is high and the river system is old, angle  $\alpha$  would be small, and whenever the migration rate is low and the river

system is young, angle  $\alpha$  would be large. Another hypothesis is that there is a relationship between angle  $\alpha$  and  $W^*$ . This would mean whenever  $W^*$  is large angle  $\alpha$  would be small and whenever  $W^*$  is small angle  $\alpha$  would be large. Testing these hypotheses is a topic for future research.

## **5.5 Future Work**

Future studies will apply these methods to a seismic volume as well as broadening the database to try to include a wider range of river system. Utilizing higher quality data, such as digital elevation models, will allow for a wider range of to be used. For ancient river systems and viewing the channel belt in a seismic volume would be best done by calculating the sweetness attribute, the instantaneous amplitude divided by the square root of the instantaneous frequency (Armstrong et al. 2013). This data will also be used to train stochastic models to understand river kinematics even further. The statistical data collected in this study will be used to train stochastic models in later research.

## **6. Conclusions**

### **6.1 Channel Belt Width**

This study has provided new knowledge by adding new constraints on the median variability of  $W^*$  is between 8.9 and 76, with a  $P_{90}/P_{10}$  ranging from 1.6-3.7. The added statistics for the channel-belt width in relation to the modern channel better show the jumping off point that helps the understanding of all other features in this study and makes early predictions about rivers not in this study.

### **6.2 Spacing of Unconformable Points**

The spacing of unconformable points has proved to be a valuable measure for gleaning insight on the evolution of channel belts and overlapping tendencies differently aged flow paths.



This discovery will be able to assist geophysicist and reservoir engineers better understand and calculate meandering fluvial reservoirs when viewing channel belts in seismic volumes.

However, given the data set in this study I have found a median range of  $L^*$  values of 2.7 to 24, with a  $P_{90}/P_{10}$  range of 2.9-7.6.

### **6.3 Radius of Curvature of Channel-Belts and Channels**

This measurement is distinctly different than similar past studies and in good way. By plotting the distribution for the radius of curvature of the channel belt edge the features can be compared easily with the other features in this study as well as be able to see more than just selected ideal meander bends. Measuring and plotting this way allows for the channel-belt to easily be compared to the modern channel. This comparison has established a median range of 3.8 to 35 with a  $P_{90}/P_{10}$  range of 16 to 49.

The ratio between the radiuses of curvature on the channel-belt to the modern channel was found to be quite close to 1:1. The importance of this is that the characteristics of the modern channel are similar to that of the channel at other times in the past. Since the channel characteristics are generally found to be similar, in the future details about a channel-belt can be estimated when only the channel is visible and vice versa.

### **6.4 Relationships Between Channel Belt Morphology and Angle $\alpha$**

The ratio  $L_{50}/P_{50}$  allows for the calculation of angle  $\alpha$ , which has a range from 29.7° to 148°. While the precise meaning of angle  $\alpha$  is unclear, it potentially provides a useful metric for quantitatively describing channel belt geometry.

### Works Cited

- Alford, John J., and Joseph C. Holmes. 1985. "Meander Scars As Evidence of Major Climate Change in Southwest Louisiana." *Annals of the Association of American Geographers* 75 (3): 395–403.
- Armstrong, Christopher, David Mohrig, Thomas Hess, Terra George, and Kyle M. Straub. 2014. "Influence of Growth Faults on Coastal Fluvial Systems: Examples from the Late Miocene to Recent Mississippi River Delta." *Sedimentary Geology* 301 (March): 120–32. doi:10.1016/j.sedgeo.2013.06.010.
- Blum, Michael D., and Jill Hattier-Womack. 2009. "Climate Change, Sea-Level Change, And Fluvial Sediment Supply To Deepwater Depositional Systems." *SEPM*, 15–39.
- Blum, Michael D., Robert A. Morton, and James M. Durbin. 1995. "AAPG Datapages/Archives: 'Deweyville' Terraces and Deposits of the Texas Gulf Coastal Plain." <http://archives.datapages.com/data/gcags/data/045/045001/0053.htm>.
- Blum, Michael D., and Torbjörn E. Törnqvist. 2000. "Fluvial Responses to Climate and Sea-Level Change: A Review and Look Forward." *Sedimentology* 47 (February): 2–48.
- Brice, James C. 1974. "Evolution of Meander Loops." *Geological Society of America Bulletin* 85 (4): 581–86. doi:10.1130/0016-7606(1974)85<581:EOML>2.0.CO;2.
- Dong, Tian Y., Jeffrey A. Nittrouer, Elena Il'icheva, Maksim Pavlov, Brandon McElroy, Matthew J. Czapiga, Hongbo Ma, and Gary Parker. 2016. "Controls on Gravel Termination in Seven Distributary Channels of the Selenga River Delta, Baikal Rift Basin, Russia." *Geological Society of America Bulletin*, B31427–1.
- Friedkin, Joseph F. 1945. "Laboratory Study of the Meandering of Alluvial Rivers." <http://agris.fao.org/agris-search/search.do?recordID=US201300197502>.
- Gibling, Martin R. 2006. "Width and Thickness of Fluvial Channel Bodies and Valley Fills in the Geological Record: A Literature Compilation and Classification." *Journal of Sedimentary Research* 76 (5): 731–70. doi:10.2110/jsr.2006.060.
- Hickin, Edward J. 1974. "The Development of Meanders in Natural River-Channels." *American Journal of Science* 274 (4): 414–42. doi:10.2475/ajs.274.4.414.
- Hickin, Edward J., and Gerald C. Nanson. 1984. "Lateral migration rates of river bends." *Journal of Hydraulic Engineering* 110.11 : 1557-1567.
- Howard, Alan D., and Thomas R. Knutson. 1984. "Sufficient Conditions for River Meandering: A Simulation Approach." *Water Resources Research* 20 (11): 1659–67. doi:10.1029/WR020i011p01659.
- Jefferson, Mark. 1902. *Limiting width of meander belts*. National Geographic Society.

- Leopold, Luna B., and M. Gordon Wolman. 1960. "River Meanders." *Geological Society of America Bulletin* 71 (6): 769–93. doi:10.1130/0016-7606(1960)71[769:RM]2.0.CO;2.
- Limaye, Ajay B. S., and Michael P. Lamb. 2014. "Numerical Simulations of Bedrock Valley Evolution by Meandering Rivers with Variable Bank Material." *Journal of Geophysical Research: Earth Surface* 119 (4): 2013JF002997. doi:10.1002/2013JF002997.
- Martin, John, Alessandro Cantelli, Chris Paola, Michael Blum, and Matthew Wolinsky. 2011. "Quantitative Modeling of the Evolution and Geometry of Incised Valleys." *Journal of Sedimentary Research* 81 (1): 64–79. doi:10.2110/jsr.2011.5.
- Martin, J.H., 1993. "A review of braided fluvial hydrocarbon reservoirs: the petroleum engineer's perspective." *Geological Society, London, Special Publications*, 75(1), pp.333-367.
- North, C. P. 1996. The prediction and modelling of subsurface fluvial stratigraphy. *Advances in fluvial dynamics and stratigraphy*, 395-508.
- Peyret, Aymeric-Pierre Bernard. 2011. "Morphodynamics and Geometry of Channels, Turbidites, and Bedforms." [Austin, Tex: University of Texas. <https://repositories.lib.utexas.edu/bitstream/handle/2152/ETD-UT-2011-12-4615/PEYRET-DISSERTATION.pdf>.
- Saucier, Roger T. 1994. *Geomorphology and Quaternary Geologic History of the Lower Mississippi Valley*. US Army Corps of Engineers.
- Saucier, R.T., 2006. *Geomorphology and quaternary geologic history of the Lower Mississippi Valley*. Storming Media.
- Stølum, Hans-Henrik. 1998. "Planform Geometry and Dynamics of Meandering Rivers." *Geological Society of America Bulletin* 110 (11): 1485–98.
- Williams, Garnett P. 1986. "River Meanders and Channel Size." *Journal of Hydrology* 88 (1): 147–64. doi:10.1016/0022-1694(86)90202-7.
- Wolman, M.G. and Leopold, L.B., 1957. *River flood plains; some observations on their formation* (No. 282-C).

## Appendix

### 1. Table of Useful Variables

<b>Variable</b>	<b>Description</b>	<b>Units</b>
$W$	Width	Meters
$W_{MC}$	Geometric mean channel width	Meters
$W_{CB}$	Channel belt width	Meters
$W_{MB}$	Meander belt width	
$W^*$	Normalized channel belt width	Dimensionless
$L$	Spacing of unconformable points	Meters
$L^*$	Normalized spacing of unconformable points	Dimensionless
$P$	Radius of Curvature	Meters
$P_C$	Radius of curvature on channel	Meters
$P_{CB}$	Radius of curvature on channel belt	Meters
$P^*$	Normalized radius of curvature	Dimensionless
$\alpha$	Meander angle arc on channel belt	Degrees

Table showing all variables within this study brief descriptions and the units associated with them.